processes

MDPI

Article

Granularity-Aware Capacity Planning of Alkaline and PEM Electrolyzers Under Heterogeneous Operating Stress

Jianguo Zhu [1], Huimin Hu [1], Zhiyin Zhang [1], Lingwen Zeng [1], Shan Li [2], Jiatong Li [3], Yuhui Lu [3], Yiwei Qiu [3,*], Shanshan Xu [4] and Zhicheng Qi [4]

[1] POWERCHINA Hubei Electric Engineering Corporation Limited, Wuhan 430040, China; zhujgsj@powerchina-hb.com (J.Z.); emyhoo@163.com (H.H.); zhangzysj@powerchina-hb.com (Z.Z.); zenglwsj@powerchina-hb.com (L.Z.)
[2] Department of Electrical Engineering, Tsinghua University, Beijing 100084, China; shanli1@mail.tsinghua.edu.cn
[3] College of Electrical Engineering, Sichuan University, Chengdu 610065, China; lijiatong@stu.scu.edu.cn (J.L.); luyh1113@163.com (Y.L.)
[4] POWERCHINA Beijing Engineering Corporation Limited, Beijing 100024, China; xuss@bjy.powerchina.cn (S.X.); qizc@bjy.powerchina.cn (Z.Q.)
* Correspondence: ywqiu@scu.edu.cn

Abstract

Off-grid renewable power-to-hydrogen (ReP2H) systems require coordinated capacity planning and operation of alkaline (ALK) and proton exchange membrane (PEM) electrolyzers. This study develops a mixed-integer linear programming model that jointly optimizes candidate-unit capacity, production–standby–idle states, and a technology-specific operating-stress proxy. The objectives combine net annualized cost, wind curtailment, and operating stress. For the 60 MW baseline operating day, the model selects 55 MW of ALK and 1 MW of PEM capacity, with 99.36% wind-power utilization and an electrolyzer-side levelized cost of hydrogen of 2.6864 CNY kg^{-1}. This value excludes wind generation, compression, storage, water treatment, and other balance-of-plant costs. Stress-aware scheduling mainly changes unit dispatch, whereas standby reduces ALK switching. The unit-level module-size, capital-cost, and objective-weight comparisons associate the small baseline PEM share with discrete capacity increments and the tested economic preferences. With the baseline capacity fixed, the continuous full-year three-state simulation produces 3.0750×10^6 kg of hydrogen with 99.429% wind-power utilization at an electrolyzer-side cost of 3.3104 CNY kg^{-1} and reduces ALK startups by 29.25% relative to the two-state model. These results delimit the operating and scenario conditions under which the reported hybrid configuration applies.

Keywords: renewable power-to-hydrogen (ReP2H); alkaline electrolyzer; proton exchange membrane electrolyzer; capacity configuration; operating stress; mixed-integer linear programming (MILP)

Check for updates

Academic Editor: Mattia Bartoli

Received: 11 September 2026
Revised: 21 October 2026
Accepted: 29 October 2026
Published: 1 November 2026

Copyright: © 2026 by the authors. Licensee MDPI, Basel, Switzerland. This article is an open access article distributed under the terms and conditions of the Creative Commons Attribution (CC BY) license.

1. Introduction

1.1. Background and Motivation

Large-scale electrification of ammonia and methanol production can contribute substantially to industrial decarbonization; however, its interaction with renewable generation must be carefully coordinated to avoid increasing power-system balancing requirements and security risks [1]. Against this background, the installed capacity of wind and solar power continues to increase as energy systems shift toward low-carbon generation.

Nevertheless, the variability and uncertainty of renewable generation complicate power balancing and energy utilization [2,3]. Renewable power-to-hydrogen (ReP2H) production provides a promising means of converting otherwise curtailed electricity into a storable and transportable energy carrier [4–7].

Alkaline electrolyzers (ALKs) are technologically mature, available at large ratings, and cost-effective, but their low-load and dynamic response capabilities are limited. Proton exchange membrane electrolyzers (PEMs), in contrast, offer wider operating ranges and faster response, making them better suited to variable renewable generation, although at a higher investment cost. High-current and dynamic operation may also introduce additional degradation stress [5,8–10]. Combining the two technologies may therefore balance cost and flexibility.

Capacity configuration, however, affects more than installed cost. It also determines how individual units are started, idled, loaded, and cycled under renewable-power fluctuations. These operating patterns can impose different stresses on ALK and PEM units and ultimately affect their long-term operation. Capacity planning should therefore be coordinated with unit-level operation and technology-specific operating stress.

1.2. Literature Review and Research Gaps

Existing studies can be divided into three areas: capacity planning for ReP2H systems, electrolyzer operating characteristics and degradation, and coordinated operation of hybrid electrolyzers.

Research on renewable hydrogen planning has evolved from equipment sizing and economic dispatch toward joint optimization over electrolyzer capacity and operation [4–7,11–13]. Cooper et al. [14] developed a design and operation framework for large wind-to-hydrogen plants and showed that renewable power profiles influence electrolyzer selection and module sizing. Sharifzadeh et al. [15] used mixed-integer linear programming (MILP) to examine the effects of minimum load, shutdown, operation above rated power, and energy storage on system economics. Other studies have considered uncertainty in investment cost, efficiency, and lifetime [16,17]. Lin et al. [18] directly optimized ALK and PEM capacities in a hybrid system, while Campbell-Stanway et al. [19] incorporated degradation costs and showed that neglecting degradation can underestimate long-term hydrogen production costs.

A second group of studies has examined technology-specific operating characteristics, including efficiency, load range, response speed, thermal behavior, gas-purity constraints, and degradation [8,9,20–26]. For ALKs, gas crossover, thermal dynamics, and hydrogen-to-oxygen (HTO) impurity limits can restrict flexibility under variable power [23,25–28]. PEMs can provide wider operating ranges and faster response [10,29], but their degradation is dominated by the membrane, catalyst layer, and porous transport layer, as well as temperature, current density, and operating mode [30–33]. Experimental studies further indicate that their effects depend on the operating condition, making a single fixed lifetime-loss coefficient inadequate for comparing different scheduling trajectories. This motivates the technology-specific operating-stress indicators proposed in this paper.

Related work has also examined multi-electrolyzer scheduling under temporally correlated renewable uncertainty, active and reactive power coordination, grid-forming energy-storage sizing, rectifier investment portfolios, and dynamic modeling and control of multi-stack alkaline electrolysis systems [34–38]. Recent studies have further considered multi-state operation of hybrid ALK/PEM systems. Ma et al. [39] modeled production, standby, and idle states together with hot and cold starts. Cheng et al. [40] studied coordinated power allocation between ALKs and PEMs while accounting for their different dynamics and state transitions. Ling et al. [41] proposed a two-stage method for hybrid capacity planning

and operation and used three-state operation and unit rotation to reduce repeated startups. Chen et al. [42] developed a robust multi-state model for multi-electrolyzer systems under wind uncertainty. Collectively, these studies show that capacity, unit states, and operating characteristics are closely coupled [39–43].

Despite these advances, three issues remain insufficiently addressed. First, continuous-capacity or aggregate-equivalent models emphasize total capacity, leaving discrete module sizes, unit-level investment decisions, and individual state transitions outside the formulation. Second, multi-state operation studies commonly assume fixed installed capacities; the effects of ALK low-load stress and PEM high-load stress on technology selection and unit numbers remain to be quantified. Third, explanations of hybrid ALK/PEM configurations often emphasize technological complementarity, and the separate contributions of operating flexibility, capital cost, and discrete module size merit further analysis. The conditions favoring a small PEM share therefore warrant systematic assessment.

1.3. Contributions of This Work

This paper develops a joint ALK/PEM capacity configuration and operation model that explicitly considers technology-specific operating stress and module-size granularity. The main contributions are as follows:

1. An MILP model is developed in which each candidate electrolyzer is represented individually. Investment, production–standby–idle states, startup and shutdown transitions, and input power are optimized simultaneously, allowing discrete module sizes and unit-level operating decisions to be captured directly.
2. Technology-specific operating-stress indices are formulated. Startup, shutdown, and load variation are considered for both ALKs and PEMs; ALK low-load operation and PEM high-load operation are also represented. These indices are incorporated into the planning model to assess how stress-aware operation affects dispatch and capacity selection.
3. The formation of hybrid configurations is examined through controlled operating-model comparisons, equal-hydrogen tests, matched module-size cases, multi-day capacity checks, and parameter-sensitivity analyses. These comparisons distinguish technology-dependent operating effects from discrete capacity-step effects.

The rest of this paper is organized as follows: Section 2 presents the hybrid electrolysis system and the technology-specific operating-stress model. Section 3 develops the multi-objective configuration and operation model and its solution method. Section 4 presents the case studies and sensitivity analyses. Section 5 concludes the paper.

2. Modeling of Hybrid Electrolysis System with Heterogeneous Operating Stresses

2.1. System Model and Assumptions

This study considers an off-grid ReP2H system comprising a wind farm, an alkaline electrolyzer (ALK) cluster, a proton exchange membrane electrolyzer (PEM) cluster, and a hydrogen outlet, as shown in Figure 1. Wind power is supplied directly to the electrolyzers, and surplus power is curtailed. Each cluster consists of candidate units with identical specifications. An installed unit can operate in production, standby, or idle mode. The model jointly determines installed units, operating states, and input power to balance system cost, wind curtailment, and operating stress.

Previous studies published in *Processes* have modeled renewable hydrogen production at both the system and device levels. System-level formulations have considered system scalability, renewable-power allocation, and electrolyzer startup and standby

characteristics [39,44]. At the device level, the static and dynamic electrical response, electrothermal coupling, mass-transport losses, and multiphase behavior of PEM and alkaline electrolyzers have been described using equivalent-circuit, macroscopic, and CFD models [45–48]. These studies provide the physical basis for distinguishing technology-dependent operating limits. Building on them, the present study adopts a planning-oriented formulation that integrates discrete unit investment, three-state operation, and technology-specific operating stress within a unified MILP framework.

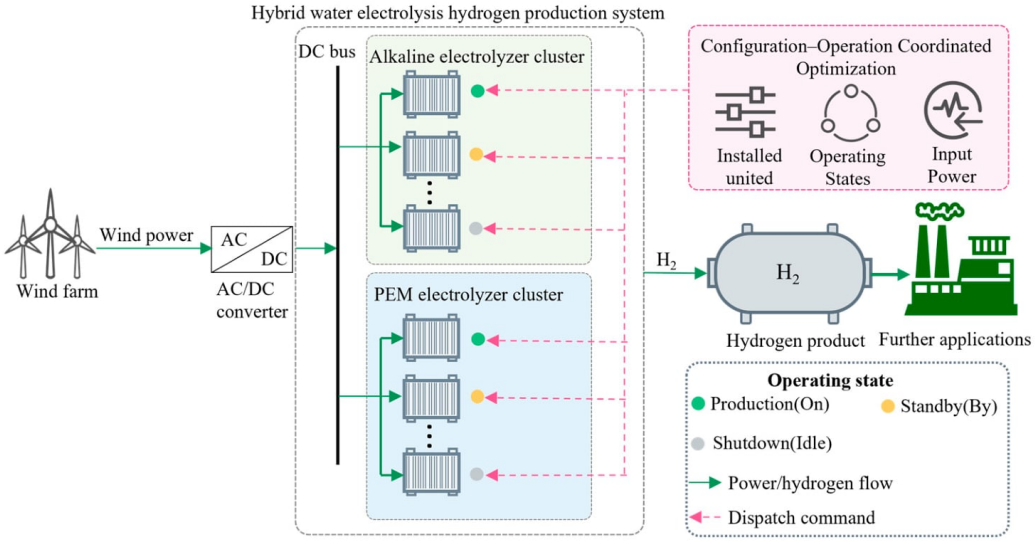

Figure 1. Schematic of the hybrid electrolysis hydrogen production system.

Let S denote the set of representative scenarios, T the set of scheduling periods, and I^{A} and I^{P} the sets of candidate ALK and PEM units, respectively. For scenario s and period t, $P^{\mathrm{w}}_{s,t}$ and $P^{\mathrm{curt}}_{s,t}$ denote the available and curtailed wind power. The production power of ALK unit i and PEM unit j is denoted by $P^{A}_{i,s,t}$ and $P^{P}_{j,s,t}$, while their standby power consumption is denoted by $P^{\mathrm{A,By}}_{i,s,t}$ and $P^{\mathrm{P,By}}_{j,s,t}$.

The utilized wind power is defined as:

$$P^{\mathrm{w,use}}_{s,t} = P^{\mathrm{w}}_{s,t} - P^{\mathrm{curt}}_{s,t} \tag{1}$$

The curtailed wind power satisfies:

$$0 \le P^{\mathrm{curt}}_{s,t} \le P^{\mathrm{w}}_{s,t}, \forall s \in S, t \in T. \tag{2}$$

The power balance for each scenario and period follows:

$$P^{\mathrm{w}}_{s,t} - P^{\mathrm{curt}}_{s,t} = \sum_{i \in I^{\mathrm{A}}} \left(P^{\mathrm{A}}_{i,s,t} + P^{\mathrm{A,By}}_{i,s,t} \right) + \sum_{j \in I^{\mathrm{P}}} (P^{\mathrm{P}}_{j,s,t} + P^{\mathrm{P,By}}_{j,s,t}), \forall s \in S, t \in T. \tag{3}$$

The formulation permits multiple representative scenarios. Let ω_s denote the annual weight of scenario s and Δt the duration of one scheduling period. For a continuous rate variable $X_{s,t}$, such as power or hydrogen production rate, the equivalent annual total is given by:

$$X^{\mathrm{ann}} = \sum_{s \in S} \omega_s \sum_{t \in T} X_{s,t} \Delta t. \tag{4}$$

For a discrete event variable $u_{s,t}$, such as startup or shutdown, the annual count follows:

$$N^{\mathrm{ann}} = \sum_{s \in S} \omega_s \sum_{t \in T} u_{s,t}. \tag{5}$$

When representative operating days are used, their annual weights satisfy $\sum_{s \in S} \omega_s = 365$.

For the present formulation, the following assumptions are adopted.

(1) The system is fully off-grid, with no power exchange with an external grid. Wind power not consumed by the electrolyzers or their standby auxiliaries is curtailed.

(2) Candidate units of the same ALK/PEM technology share the same rated power, operating range, standby consumption, transition constraints, and stress parameters; ALK and PEM units have technology-specific characteristics.

(3) Hydrogen produced by all units is aggregated at a common outlet and valued at a fixed price.

(4) Each 15 min scheduling period is represented by a quasi-steady operating point. Temperature, gas purity, cold/warm startup duration, transition energy, and sub-interval dynamics are not resolved explicitly. Minimum-load limits define hard operating bounds; low-/high-load terms guide schedule selection within those bounds.

2.2. Candidate-Unit Configuration and Three-State Operation

A candidate-unit formulation is used to determine both installed capacity and unit-level operation. The candidate sets are denoted by:

$$I^{\mathrm{A}} = \{1, 2, \ldots, N^{\mathrm{A}}_{\max}\}, \tag{6}$$

$$I^{\mathrm{P}} = \{1, 2, \ldots, N^{\mathrm{P}}_{\max}\}, \tag{7}$$

where $N^{\mathrm{A}}_{\max}$ and $N^{\mathrm{P}}_{\max}$ are the maximum numbers of ALK and PEM units.

The binary configuration variables for both units are:

$$y^{\mathrm{A}}_i \in \{0, 1\}, \forall i \in I^{\mathrm{A}}, \tag{8}$$

$$y^{\mathrm{P}}_j \in \{0, 1\}, \forall j \in I^{\mathrm{P}}. \tag{9}$$

A value of $y^{\mathrm{A}}_i = 1$ or $y^{\mathrm{P}}_j = 1$ indicates that the corresponding ALK or PEM unit is installed. These variables are invariant across scenarios and scheduling periods. The numbers of installed units then follow:

$$N^{\mathrm{A}} = \sum_{i \in I^{\mathrm{A}}} y^{\mathrm{A}}_i, \tag{10}$$

$$N^{\mathrm{P}} = \sum_{j \in I^{\mathrm{P}}} y^{\mathrm{P}}_j. \tag{11}$$

Let $\overline{P}^{\mathrm{A}}$ and $\overline{P}^{\mathrm{P}}$ denote the rated power of individual ALK and PEM units. The installed capacities are:

$$P^{\mathrm{A,cap}} = \overline{P}^{\mathrm{A}} N^{\mathrm{A}}, \tag{12}$$

$$P^{\mathrm{P,cap}} = \overline{P}^{\mathrm{P}} N^{\mathrm{P}}. \tag{13}$$

The total rated capacity thus follows:

$$P^{\mathrm{cap}} = P^{\mathrm{A,cap}} + P^{\mathrm{P,cap}}. \tag{14}$$

PEM units may operate above rated power within the prescribed upper bound in Section 2.3. The 1.20 p.u. value is adopted as a case-study operating bound consistent with the planning formulation in [40]. The model treats it as a power bound; duration and recovery dynamics are outside its scope. Accordingly, assessment of sustained 120% operation or technology-specific ramp-rate performance requires explicit dynamic constraints:

$$y^{\mathrm{A}}_i \geq y^{\mathrm{A}}_{i+1}, i = 1, 2, \ldots, N^{\mathrm{A}}_{\max} - 1, \tag{15}$$

$$y_j^{\mathrm{P}} \geq y_{j+1}^{\mathrm{P}}, j = 1, 2, \ldots, N_{\max}^{\mathrm{P}} - 1. \tag{16}$$

Each installed unit can be in production, standby, or idle state during operation. A production unit consumes power and produces hydrogen; a standby unit consumes auxiliary power without producing hydrogen; and an idle unit consumes neither production nor standby power. The superscripts On, By, and Idle denote these states.

The binary state variables for ALK units are:

$$b_{i,s,t}^{\mathrm{A,On}}, b_{i,s,t}^{\mathrm{A,By}}, b_{i,s,t}^{\mathrm{A,Idle}} \in \{0,1\}, \forall i \in I^{\mathrm{A}}, s \in S, t \in T, \tag{17}$$

and satisfy

$$b_{i,s,t}^{\mathrm{A,On}} + b_{i,s,t}^{\mathrm{A,By}} + b_{i,s,t}^{\mathrm{A,Idle}} = y_i^{\mathrm{A}}, \forall i \in I^{\mathrm{A}}, s \in S, t \in T, \tag{18}$$

Similarly, the binary state variables for PEM units are defined by:

$$b_{j,s,t}^{\mathrm{P,On}}, b_{j,s,t}^{\mathrm{P,By}}, b_{j,s,t}^{\mathrm{P,Idle}} \in \{0,1\}, \forall j \in I^{\mathrm{P}}, s \in S, t \in T, \tag{19}$$

with

$$b_{j,s,t}^{\mathrm{P,On}} + b_{j,s,t}^{\mathrm{P,By}} + b_{j,s,t}^{\mathrm{P,Idle}} = y_j^{\mathrm{P}}, \forall j \in I^{\mathrm{P}}, s \in S, t \in T. \tag{20}$$

Furthermore, an uninstalled unit has all state variables equal to zero. For an installed unit, exactly one state is active in each scenario and period. Thus, the state-configuration constraints directly link investment decisions to unit-level operation.

2.3. State Transitions and Hydrogen Production

Based on the three-state model, this section describes state transitions between adjacent periods, production power, standby consumption, and hydrogen output. The energized state $z_{i,s,t}^{\mathrm{A}}$ and $z_{j,s,t}^{\mathrm{P}}$ are defined as the sum of the production and standby states:

$$z_{i,s,t}^{\mathrm{A}} = b_{i,s,t}^{\mathrm{A,On}} + b_{i,s,t}^{\mathrm{A,By}}, \tag{21}$$

$$z_{j,s,t}^{\mathrm{P}} = b_{j,s,t}^{\mathrm{P,On}} + b_{j,s,t}^{\mathrm{P,By}}. \tag{22}$$

For cyclic representative scenarios, the last and first periods are linked to preserve state continuity. Let $\pi(t)$ denote the period preceding t, as:

$$\pi(t) = \begin{cases} t-1, t = 2, \ldots, |T| \\ |T|, t = 1 \end{cases}, \tag{23}$$

and the following-period index be

$$\Phi_{T(t,k)} = 1 + \mathrm{mod}(t + k - 2, |T|). \tag{24}$$

A startup occurs when a unit moves from idle to either production or standby, whereas a shutdown occurs when it moves from an energized state to idle. Let u and v denote the binary startup and shutdown variables. For ALK units, we have

$$z_{i,s,t}^{\mathrm{A}} - z_{i,s,\pi(t)}^{\mathrm{A}} = u_{i,s,t}^{\mathrm{A}} - v_{i,s,t}^{\mathrm{A}}, \tag{25}$$

$$u_{i,s,t}^{\mathrm{A}} + v_{i,s,t}^{\mathrm{A}} \leq 1, \tag{26}$$

and similarly, for PEM units:

$$z_{j,s,t}^{\mathrm{P}} - z_{j,s,\pi(t)}^{\mathrm{P}} = u_{j,s,t}^{\mathrm{P}} - v_{j,s,t}^{\mathrm{P}}, \tag{27}$$

$$u_{j,s,t}^{\mathrm{P}} + v_{j,s,t}^{\mathrm{P}} \leq 1. \tag{28}$$

Only transitions between idle and energized states are counted as startups or shutdowns.

To represent the slower restart characteristics of ALK units, a minimum idle duration is imposed after shutdown. Let $T^{\mathrm{A}}_{\mathrm{idle}}$ denote the required number of consecutive idle periods. The constraint is:

$$\sum_{k=0}^{T^{\mathrm{A}}_{\mathrm{Idle}}-1} b^{\mathrm{A,Idle}}_{i,s,\Phi_{T(t,k)}} \geq T^{\mathrm{A}}_{\mathrm{Idle}} v^{\mathrm{A}}_{i,s,t}. \tag{29}$$

The variables $P^{\mathrm{A}}_{i,s,t}$ and $P^{\mathrm{P}}_{j,s,t}$ represent the total AC-side input power of units in production, including auxiliary power $P^{\mathrm{A,By}}_{i,s,t}$ and $P^{\mathrm{P,By}}_{j,s,t}$ required during hydrogen production. The ALK production power satisfies:

$$\underline{P}^{\mathrm{A}} b^{\mathrm{A,On}}_{i,s,t} \leq P^{\mathrm{A}}_{i,s,t} \leq \overline{P}^{\mathrm{A}} b^{\mathrm{A,On}}_{i,s,t}, \tag{30}$$

and for PEM units:

$$\underline{P}^{\mathrm{P}} b^{\mathrm{P,On}}_{j,s,t} \leq P^{\mathrm{P}}_{j,s,t} \leq \overline{P}^{\mathrm{P,run}} b^{\mathrm{P,On}}_{j,s,t}, \tag{31}$$

where $\underline{P}^{\mathrm{A}}$ and $\underline{P}^{\mathrm{P}}$ are the minimum production powers; $\overline{P}^{\mathrm{A}}$ and $\overline{P}^{\mathrm{P}}$ are the rated powers of one ALK and one PEM unit. The maximum PEM operating power is:

$$\overline{P}^{\mathrm{P,run}} = \alpha^{\mathrm{P}}_{\max} \overline{P}^{\mathrm{P}}, \tag{32}$$

where $\alpha^{\mathrm{P}}_{\max}$ denotes the maximum operating power factor.

A unit in standby produces no hydrogen but consumes auxiliary power to maintain required operating conditions. Let $\rho^{\mathrm{A}}_{\mathrm{By}}$ and $\rho^{\mathrm{P}}_{\mathrm{By}}$ denote the standby power ratios. The standby consumption is:

$$P^{\mathrm{A,By}}_{i,s,t} = \rho^{\mathrm{A}}_{\mathrm{By}} \overline{P}^{\mathrm{A}} b^{\mathrm{A,By}}_{i,s,t}, \tag{33}$$

$$P^{\mathrm{P,By}}_{j,s,t} = \rho^{\mathrm{P}}_{\mathrm{By}} \overline{P}^{\mathrm{P}} b^{\mathrm{P,By}}_{j,s,t}. \tag{34}$$

In idle mode, both production and standby power are zero. Substituting the production and standby terms into the power-balance equation in Section 2.1 gives the equality constraints between utilized wind power and total system demand.

To preserve linearity, hydrogen production is represented by constant conversion coefficients [23]. This planning approximation neglects load-, temperature-, and age-dependent efficiency. This simplification may affect the relative value of part-load operation and is treated as a limitation of the planning model. The coefficient-equalization test in Section 4.5 examines one bounded aspect of this assumption; nonlinear efficiency-curve analysis remains outside the present planning framework:

$$m^{\mathrm{A}}_{i,s,t} = \alpha^{\mathrm{A}}_{\mathrm{H_2}} P^{\mathrm{A}}_{i,s,t} \Delta t, \tag{35}$$

$$m^{\mathrm{P}}_{j,s,t} = \alpha^{\mathrm{P}}_{\mathrm{H_2}} P^{\mathrm{P}}_{j,s,t} \Delta t, \tag{36}$$

The annual hydrogen production is therefore:

$$\mathrm{H}_{2,\mathrm{year}} = \sum_{s \in S} \omega_s \sum_{t \in T} \Big(\sum_{i \in I^{\mathrm{A}}} m^{\mathrm{A}}_{i,s,t} + \sum_{j \in I^{\mathrm{P}}} m^{\mathrm{P}}_{j,s,t} \Big), \tag{37}$$

where ω_s is the annual weight of scenario s.

2.4. Technology-Specific Operating-Stress Model

ALK and PEM electrolyzers differ in operating limits and in their qualitative sensitivity to switching, power variation, and load region. The following terms therefore form a relative operating-stress proxy for comparing schedules. The index is a scheduling proxy for comparing operating plans; voltage loss, efficiency decay, remaining life, and replacement cost are outside its scope.

Specifically, for technology $k \in K = \{\mathrm{A},\mathrm{P}\}$, let $\Delta P^{k}_{i,s,t}$ denote the absolute change in the production power of candidate unit i between two adjacent periods as:

$$\Delta P^{k}_{i,s,t} \geq P^{k}_{i,s,t} - P^{k}_{i,s,\pi(t)}, \tag{38}$$

$$\Delta P^{k}_{i,s,t} \geq P^{k}_{i,s,\pi(t)} - P^{k}_{i,s,t}, \tag{39}$$

$$\Delta P^{k}_{i,s,t} \geq 0, \forall i \in I^{k},\ s \in S,\ t \in T. \tag{40}$$

When power variation has a positive coefficient in the scalar objective, these constraints yield:

$$\Delta P^{k}_{i,s,t} = \left| P^{k}_{i,s,t} - P^{k}_{i,s,\pi(t)} \right|. \tag{41}$$

Power variation is calculated for each unit as the sum of adjacent-period absolute MW changes. The unit-level formulation sums each device's absolute change, so movements in opposite directions remain additive. The annualized quantity retains the unit MW because it is a discrete total variation, not an energy integral; the factor Δt enters the dimensionless stress component. Internal redispatch among identical units can nevertheless create label-dependent variation, so Section 4.3 reports both unit-level and technology-aggregate totals.

2.4.1. ALK Operating Stress

ALK operation below a specified load threshold remains feasible but incurs a scheduling penalty. The hard minimum-load constraint represents the admissible operating boundary, whereas the low-load term expresses a relative preference motivated by gas-crossover and lye-circulation concerns [25–28]. This term represents a scheduling preference; HTO safety constraints and calibrated degradation rates are outside its definition:

$$P^{\mathrm{A}}_{\mathrm{stress}} = \alpha^{\mathrm{A}}_{\mathrm{stress}} \overline{P}^{\mathrm{A}}. \tag{42}$$

which is set above the minimum feasible production load. Therefore, operation between the minimum load and the stress threshold is still allowed but contributes to the low-load term.

Let $L^{\mathrm{A}}_{i,s,t}$ denote the ALK low-load deviation:

$$L^{\mathrm{A}}_{i,s,t} \geq P^{\mathrm{A}}_{\mathrm{stress}} b^{\mathrm{A,On}}_{i,s,t} - P^{\mathrm{A}}_{i,s,t}, \tag{43}$$

$$L^{\mathrm{A}}_{i,s,t} \geq 0. \tag{44}$$

which is zero when the unit is idle, in standby, or operates above the threshold, and increases as production power falls below it.

The ALK operating-stress index is thus defined as:

$$D^{\mathrm{A}} = \frac{1}{D_{\mathrm{ref}}} \sum_{s \in S} \omega_s \sum_{t \in T} \sum_{i \in I^{\mathrm{A}}} \left[\gamma^{\mathrm{A}}_{\mathrm{start}} \overline{P}^{\mathrm{A}} u^{\mathrm{A}}_{i,s,t} + \gamma^{\mathrm{A}}_{\mathrm{stop}} \overline{P}^{\mathrm{A}} v^{\mathrm{A}}_{i,s,t} + \gamma^{\mathrm{A}}_{\Delta P} \Delta P^{\mathrm{A}}_{i,s,t} + \gamma^{\mathrm{A}}_{\mathrm{load}} L^{\mathrm{A}}_{i,s,t} \right] \Delta t, \tag{45}$$

where $\gamma^{\mathrm{A}}_{\mathrm{start}}$, $\gamma^{\mathrm{A}}_{\mathrm{stop}}$, $\gamma^{\mathrm{A}}_{\Delta P}$, and $\gamma^{\mathrm{A}}_{\mathrm{load}}$ are the relative weights assigned to startup, shutdown, power variation, and low-load operation, respectively.

2.4.2. PEM Operating Stress

PEM operation above the nominal rating contributes to a high-load stress term up to the model upper bound. The threshold separates nominal and above-nominal operation for scheduling purposes; it is not a universal material-failure threshold:

$$P^{\mathrm{P}}_{\mathrm{stress}} = \alpha^{\mathrm{P}}_{\mathrm{stress}} \overline{P}^{\mathrm{P}}. \tag{46}$$

The maximum feasible operating power is subject to:

$$P^{\mathrm{P}}_{j,s,t} \leq \alpha^{\mathrm{P}}_{\mathrm{max}} \overline{P}^{\mathrm{P}} b^{\mathrm{P,On}}_{j,s,t}, \tag{47}$$

where $\alpha^{\mathrm{P}}_{\max}$ is the maximum operating-power factor.

Let $H^{\mathrm{P}}_{j,s,t}$ denote the high-load deviation, as

$$H^{\mathrm{P}}_{j,s,t} \geq P^{\mathrm{P}}_{j,s,t} - P^{\mathrm{P}}_{\mathrm{stress}} b^{\mathrm{P,On}}_{j,s,t}, \tag{48}$$

$$H^{\mathrm{P}}_{j,s,t} \geq 0. \tag{49}$$

This term is zero at or below the high-load threshold and increases with the excess power above it.

The PEM operating-stress index is thus summarized as

$$D^{\mathrm{P}} = \frac{1}{D_{\mathrm{ref}}} \sum_{s \in S} \omega_s \sum_{t \in T} \sum_{j \in I^{\mathrm{P}}} \left[\gamma^{\mathrm{P}}_{\mathrm{start}} \overline{P}^{\mathrm{P}} u^{\mathrm{P}}_{j,s,t} + \gamma^{\mathrm{P}}_{\mathrm{stop}} \overline{P}^{\mathrm{P}} v^{\mathrm{P}}_{j,s,t} + \gamma^{\mathrm{P}}_{\Delta P} \Delta P^{\mathrm{P}}_{j,s,t} + \gamma^{\mathrm{P}}_{\mathrm{load}} H^{\mathrm{P}}_{j,s,t} \right] \Delta t. \tag{50}$$

The total system operating-stress index is:

$$D_{sys} = D^{\mathrm{A}} + D^{\mathrm{P}}. \tag{51}$$

A fixed reference scale is used to make the index dimensionless:

$$D_{\mathrm{ref}} = P_{\mathrm{ref}} T_{\mathrm{ref}} N_{\mathrm{day}}, \tag{52}$$

where P_{ref}, T_{ref} and N_{day} denote the fixed reference power, duration, and annualization factor, respectively.

In the optimization, startup and shutdown are weighted by unit rated capacity, while power variation and low-/high-load terms use the corresponding MW deviations. Previous studies describe alkaline flexibility limits associated with gas purity and process dynamics, and report condition-dependent effects of dynamic PEM operation on performance and degradation [9,25,26,29,31–33]. These studies motivate the selected stress components and their technology-specific representation. They report no numerical coefficients transferable to the present normalized scheduling objective. The numerical coefficients adopted in the case study are engineering-selected relative weights informed by the qualitative literature trends; calibration against experimental degradation or lifetime data remains future work. Each coefficient is varied individually in Section 4.7. Because event and variation terms are evaluated on the 15 min grid, the absolute index is resolution-specific, and its coefficients must be recalibrated if Δt changes.

3. Multi-Objective Optimization Model for Joint Capacity Configuration and Operation

The unit-level configuration, operating state, hydrogen production, and operating-stress models developed in Section 2 are integrated here into a multi-objective planning framework. Capacity configuration and scenario-dependent operation are optimized simultaneously to balance economic performance, wind curtailment, and operating stress.

3.1. Joint Capacity and Operation Framework

The decision variables consist of scenario-independent configuration variables and scenario-dependent operating variables. The configuration vector is thus formulated as

$$x = \left\{ y^{\mathrm{A}}_i, y^{\mathrm{P}}_j \middle| i \in I^{\mathrm{A}}, j \in I^{\mathrm{P}} \right\}, \tag{53}$$

where y^{A}_i and y^{P}_j indicate whether ALK unit i and PEM unit j are installed. The vector x determines the number and rated capacity of both technologies. All representative scenarios share the same configuration.

The variable domains, ordering constraints, and capacity relations in Section 2.2 define the feasible configuration set:

$$x \in \chi^{\mathrm{cfg}} \tag{54}$$

For each scenario s, the model determines the operating states and power allocation of the installed units. Let $K = \{\mathrm{A},\mathrm{P}\}$ denote the set of electrolyzer technologies. The three operating states of technology k are represented by:

$$b_s^k = \left\{ b_s^{k,\mathrm{On}}, b_s^{k,\mathrm{By}}, b_s^{k,\mathrm{Idle}} \right\}. \tag{55}$$

The scenario-dependent operating vector is summarized:

$$q_s = \bigcup_{k \in K} \left\{ b_s^k, u_s^k, v_s^k, P_s^k, m_s^k, \Delta P_s^k \right\} \cup \left\{ L_s^A, H_s^P, P_s^{\mathrm{curt}} \right\} \tag{56}$$

where u_s^k and v_s^k denote startup and shutdown decisions; P_s^k and m_s^k represent production power and hydrogen output, and ΔP_s^k measures power variation; L_s^{A} and H_s^{P} denote the ALK low-load deviation and PEM high-load deviation; P_s^{curt} contains the curtailed wind power for all periods in scenario s.

The constraints in Section 2 define the feasible operating set for each scenario:

$$q_s \in \Omega_s(x), \forall s \in S \tag{57}$$

The resulting annual performance vector is defined as:

$$\mathrm{F} = (f_{\mathrm{C}}, f_{\mathrm{curt}}, f_{\mathrm{D}}) = \left(C_{\mathrm{net}}, E_{\mathrm{curt}}, D_{\mathrm{sys}} \right) \tag{58}$$

where C_{net}, E_{curt}, and D_{sys} denote net annualized cost, curtailed wind energy, and the operating stress index.

3.2. Objective Functions and Multi-Objective Coordination

The optimization considers three objectives: net annualized cost, wind curtailment, and operating stress. Fixed reference scales are used to combine them in a weighted scalar objective. The LCOH is evaluated separately after optimization.

The annualized electrolyzer cost before hydrogen revenue is:

$$C_{\mathrm{ann}} = C_{\mathrm{inv}} + C_{\mathrm{om}} + C_{\mathrm{ss}}, \tag{59}$$

where C_{inv}, C_{om}, and C_{ss} denote the annualized investment cost, fixed operation and maintenance cost, and startup and shutdown cost, respectively.

The annualized investment cost is:

$$C_{\mathrm{inv}} = \sum_{k \in K} \mathrm{CRF}^k c_{\mathrm{inv}}^k P_{\mathrm{cap}}^k, \tag{60}$$

where c_{inv}^k is the investment cost per unit capacity; and P_{cap}^k is the installed rated capacity of technology k. The capital recovery factor is thus:

$$\mathrm{CRF}^k = \frac{r(1+r)^{n^k}}{(1+r)^{n^k} - 1}, \tag{61}$$

where r is the discount rate and n^k is the economic lifetime of technology k.

The annual fixed operation and maintenance cost is:

$$C_{\mathrm{om}} = \sum_{k \in K} c_{\mathrm{om}}^k P_{\mathrm{cap}}^k, \tag{62}$$

where c_{om}^k is the annual fixed O&M cost per unit installed capacity.

Annual startup and shutdown cost is:

$$C_{\mathrm{ss}} = \sum_{s\in S} \omega_s \sum_{t\in T} \sum_{k\in K} \sum_{i\in I^k} \left(c^k_{\mathrm{start}} u^k_{i,s,t} + c^k_{\mathrm{stop}} v^k_{i,s,t} \right), \tag{63}$$

where c^k_{start} and c^k_{stop} denote the cost of one startup and shutdown event, respectively.

Annual hydrogen sales revenue is calculated as:

$$R_{\mathrm{H_2}} = p_{\mathrm{H_2}} \mathrm{H}_{2,\mathrm{year}} \tag{64}$$

where $p_{\mathrm{H_2}}$ is the hydrogen price; and $\mathrm{H}_{2,\mathrm{year}}$ is annual hydrogen production. The net annualized cost used is therefore:

$$C_{\mathrm{net}} = C_{\mathrm{ann}} - R_{\mathrm{H_2}}. \tag{65}$$

The electrolyzer-side LCOH is calculated after optimization as:

$$LCOH_{\mathrm{el}} = \frac{C_{\mathrm{ann}}}{H_{2,\mathrm{year}}}. \tag{66}$$

The reported $LCOH_{\mathrm{el}}$ covers annualized electrolyzer investment, fixed O&M, and switching costs within the electrolyzer-side system boundary.

The annual curtailed wind energy is:

$$E_{\mathrm{curt}} = \sum_{s\in S} \omega_s \sum_{t\in T} P^{\mathrm{curt}}_{s,t} \Delta t. \tag{67}$$

The three system-level objectives are therefore defined as:

$$f_{\mathrm{C}} = C_{\mathrm{net}}, \tag{68}$$

$$f_{\mathrm{curt}} = E_{\mathrm{curt}}, \tag{69}$$

$$f_{\mathrm{D}} = D_{\mathrm{sys}}. \tag{70}$$

Because these objectives have different units and magnitudes, fixed reference scales are introduced. The normalized economic objective is:

$$\hat{f}_{\mathrm{C}} = \frac{C_{\mathrm{net}}}{C_{\mathrm{ref}}} \tag{71}$$

where C_{ref} is a fixed numerical scaling parameter, independent of cost bounds and the optimized reference configuration.

The normalized renewable curtailment objective is:

$$\hat{f}_{\mathrm{curt}} = \frac{E_{\mathrm{curt}}}{E_{\mathrm{W}}}, \tag{72}$$

where E_W denotes the available wind energy over the optimization horizon.

The operating-stress objective is:

$$\hat{f}_{\mathrm{D}} = D_{\mathrm{sys}} \tag{73}$$

No additional normalization is required because D_{sys} has already been normalized using the fixed reference D_{ref} in Section 2.4.

The three normalized objectives are combined as:

$$\min \Phi = w_{\mathrm{C}} \hat{f}_{\mathrm{C}} + w_{\mathrm{curt}} \hat{f}_{\mathrm{curt}} + w_{\mathrm{D}} \hat{f}_{\mathrm{D}}, \tag{74}$$

subject to

$$w_{\mathrm{C}} + w_{\mathrm{curt}} + w_{\mathrm{D}} = 1, \tag{75}$$

$$w_C, w_{curt}, w_D \geq 0. \tag{76}$$

The weights determine the decision-maker's relative emphasis on economic performance, wind curtailment, and operating stress. The baseline 0.90/0.05/0.05 setting is used as a representative economics-led compromise. Section 4.5.5 evaluates nearby combinations; W3 and W4 are reported as the best feasible solutions obtained within the time limit.

The reference scales C_{ref}, E_W, and D_{ref} are fixed independently of the optimized solution. The fixed reference scales and objective weights keep all objective terms linear, preserving the MILP formulation.

3.3. MILP Formulation and Solution Method

Combining the configuration and operating constraints with the scalar objective yields the final optimization problem:

$$\min_{x,\{q_s\}_{s\in S}} \Phi = \sum_{k=1}^{3} \lambda_k \hat{f}_k, \tag{77}$$

subject to

$$x \in \chi^{cfg}, q_s \in \Omega_s(x), \forall s \in S, \tag{78}$$

In Equation (77), λ_1, λ_2, and λ_3 correspond to the cost, curtailment, and operating-stress weights defined in Equation (74), respectively; the normalized objectives are unchanged.

X^{cfg} contains the configuration variables, ordering constraints, and capacity relations defined in Section 2.2. The set $\Omega_s(x)$ contains the three-state operation, startup and shutdown, power limits, power balance, power-to-hydrogen conversion, and operating-stress constraints for scenario s.

The scenario variables are divided into binary and continuous sets:

$$q_s^{bin} = \left\{b_s^{On}, b_s^{By}, b_s^{Idle}, u_s, v_s\right\}, \tag{79}$$

$$q_s^{con} = \{P_s, m_s, \Delta P_s, L_s, H_s, P_s^{curt}\}, \tag{80}$$

$$q_s^{bin} \in \{0,1\}^{n_s^{bin}}, q_s^{con} \geq 0. \tag{81}$$

Absolute power variation and the ALK low-load and PEM high-load deviations are represented using the linear auxiliary-variable formulations introduced in Section 2.4. State selection, configuration coupling, and startup/shutdown logic are expressed through binary linear constraints; standby demand, power balance, and hydrogen production use linear relations. The complete formulation is therefore a mixed-integer linear programming model.

When the corresponding stress term has a positive weight in the scalar objective, the auxiliary variables for power variation and low- or high-load deviation attain their exact absolute-value or positive-part values. If the operating-stress weight is set to zero, these quantities are recalculated after optimization from the resulting dispatch to ensure consistent stress reporting.

4. Case Studies

4.1. Case Settings

A 60 MW off-grid wind-to-hydrogen case is used to evaluate the proposed ALK/PEM configuration and operation model. The system consists of a wind farm and ALK and PEM electrolyzer clusters. Grid exchange is excluded; available wind power is allocated among hydrogen production, standby consumption, and curtailment.

Sections 4.2–4.5 use one 24 h baseline operating day with 96 intervals at 15 min resolution. The same profile is used for controlled model comparisons, and its daily quantities are multiplied by 365 to obtain equivalent annual values under a cyclic boundary. The profile

is not claimed to represent seasonal variability or to predict a specific year. Section 4.7 explores four clustered, weighted daily profiles using an aggregate screening formulation; the scope of this approximation is stated explicitly.

Because a cyclic baseline day omits cross-day transitions, Section 4.6 evaluates the fixed baseline capacity on a continuous 35,040-point sequence. This section validates chronological operation at the baseline capacity. The four-representative-day screening in Section 4.7 provides exploratory scenario comparisons, with a different aggregation level from the unit-level model.The baseline operating-day and candidate-unit settings are summarized in Table 1.

Table 1. Baseline operating-day and candidate-unit settings.

Parameter	Symbol	Value	Unit
Rated wind-farm capacity	$P_{\mathrm{W}}^{\mathrm{rated}}$	60	MW
Time step	Δt	0.25	h
Periods in the baseline operating day	N_T	96	–
Equivalent annualization weight	ω	365	d yr^{-1}
Rated capacity of one ALK unit	$\overline{P}^{\mathrm{A}}$	5	MW unit^{-1}
Rated capacity of one PEM unit	$\overline{P}^{\mathrm{P}}$	1	MW unit^{-1}
ALK candidate number/capacity limit	$N_{\max}^{\mathrm{A}}/P_{\max}^{\mathrm{A}}$	12/60	unit/MW
PEM candidate number/capacity limit	$N_{\max}^{\mathrm{P}}/P_{\max}^{\mathrm{P}}$	60/60	unit/MW

The 20-year system economic life is consistent with published electrolyzer techno-economic assumptions [49,50], and the fixed O&M rate of 2% of initial CAPEX per year is reported in [50]. Typical design studies have also examined capacity configuration and electrolyzer equipment selection in wind–solar coupled hydrogen production systems [51]. The exact CAPEX values used in Table 2 (ALK: 1,200,000; PEM: 4,000,000 CNY/MW) remain case-study inputs because the cited studies do not verify these values as current quotations; the PEM value is also reported as a 2030 projection [52]. The hydrogen-production coefficients are likewise case-study approximations: 18.0 and 18.5 kg/MWh correspond to 55.56 and 54.05 kWh/kg, respectively, which are near system-specific electricity-consumption values reported in [49,50]. The hydrogen price of 20 CNY/kg is a scenario informed by a published Qinghai projection, not a current market price [53]. The exact startup and shutdown event costs remain case-study assumptions; published scheduling work notes that such costs require manufacturer- or operator-specific data for refinement [54]. Their effects are tested in Section 4.7. Minimum-load limits, the PEM maximum-power factor, standby-power ratios, and numerical stress weights are also case-study settings; the cited literature provides context but does not establish these exact values.The operating-stress, objective-normalization, and solver parameters are summarized in Table 3.

Table 2. Technical and economic parameters of ALK and PEM electrolyzers.

Parameter	Symbol	ALK	PEM	Unit
Minimum production-load ratio	$\alpha_{\min}^{k}$	0.25	0.05	p.u.
Maximum operating-power factor	$\alpha_{\max}^{k}$	1.00	1.20	p.u.
Standby-power ratio	ρ_{By}^{k}	0.03	0.03	p.u.
Hydrogen-production coefficient	$\alpha_{\mathrm{H_2}}^{k}$	18.0	18.5	kg MWh^{-1}
Investment cost per MW	c_{inv}^{k}	1,200,000	4,000,000	CNY MW^{-1}
Fixed O&M cost	c_{om}^{k}	24,000	80,000	CNY MW^{-1} yr^{-1}
Startup cost	c_{start}^{k}	1000	200	CNY event^{-1}
Shutdown cost	c_{stop}^{k}	200	50	CNY event^{-1}
Minimum idle time	T_{Idle}^{k}	0.5	N/A	h
Economic lifetime	n^{k}	20	20	yr

Table 3. Operating-stress, objective-normalization, and solver parameters.

Parameter	Symbol	ALK	PEM	Unit
Startup-stress weight	$\gamma^{k}_{\text{start}}$	30	8	Dimensionless
Shutdown-stress weight	γ^{k}_{stop}	10	3	Dimensionless
Power-variation stress weight	$\gamma^{k}_{\Delta P}$	20	5	Dimensionless
Low-/high-load stress weight	γ^{k}_{load}	10	5	Dimensionless
Low-/high-load stress threshold	$\alpha^{k}_{\text{stress}}$	0.40	1.00	p.u.
Discount rate	r	0.08	0.08	-
Capital recovery factor	CRF	0.10185221	0.10185221	-
Hydrogen price	p_{H_2}	20	20	CNY kg^{-1}
Fixed reference power	P_{ref}	60	60	MW
Fixed reference duration	T_{ref}	24	24	h
Stress-normalization reference	D_{ref}	525,600	525,600	MWh yr^{-1}
Cost-normalization reference scale	C_{ref}	38,017,889.15	38,017,889.15	CNY yr^{-1}
Curtailment-normalization reference	E_{W}	Available wind energy over the optimization horizon	Available wind energy over the optimization horizon	MWh
Three objective weights	$w_{\text{C}}/w_{\text{curt}}/w_{\text{D}}$	0.90/0.05/0.05	0.90/0.05/0.05	-
Relative MIP optimality gap	ε_{MIP}	1.0×10^{-5}	1.0×10^{-5}	-
Time limit per solve	T_{lim}	3600	3600	s

Note: $k \in \{A,P\}$ denotes the electrolyzer technology, where A and P represent ALK and PEM, respectively. $D_{\text{ref}} = P_{\text{ref}} T_{\text{ref}} N_{\text{day}} = 525{,}600$ MWhyr^{-1}, where $N_{\text{day}} = 365$. E_W denotes the available wind energy over the corresponding optimization horizon, and C_{ref} is a fixed reference scale used only for objective normalization.

4.2. Base Case

The base case selects 11 ALK units and one PEM unit, corresponding to 55 MW of ALK and 1 MW of PEM capacity. The candidate limits are nonbinding, and PEM therefore provides only a small supplementary share of the total 56 MW capacity.

As shown in Figure 2, the total electrolyzer load tracked the wind-power profile, with only limited curtailment required to maintain the strict off-grid power balance. The equivalent annual wind energy was 277,777.78 MWh, of which 275,986.54 MWh was utilized, corresponding to a wind-power utilization rate of 99.36% and an annualized curtailment of 1791.24 MWh. Equivalent annual hydrogen production reached 4.9686×10^6 kg. The electrolyzer-side annualized cost was $C_{\text{ann}} = 13{,}347{,}654.62$ CNY yr^{-1}, with $LCOH_{\text{el}} = 2.6864$ CNY kg^{-1}.

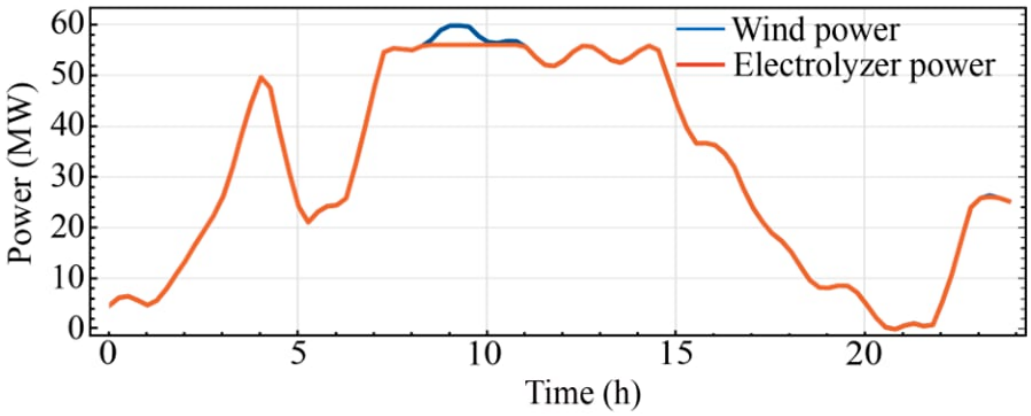

Figure 2. Wind power and electrolyzer power in the base case.

Figure 3 shows that ALK units supply most of the production load and alternate among production, standby, and idle as wind power changes. Their equivalent annual startup and

shutdown counts are both 4015, with 1186.25 unit·h of standby operation. The PEM unit operates between 0.05 and 1.20 MW without equivalent annual startup or shutdown events; in this model, it provides a fine capacity and power-allocation increment; fast–dynamic services are outside the model scope.

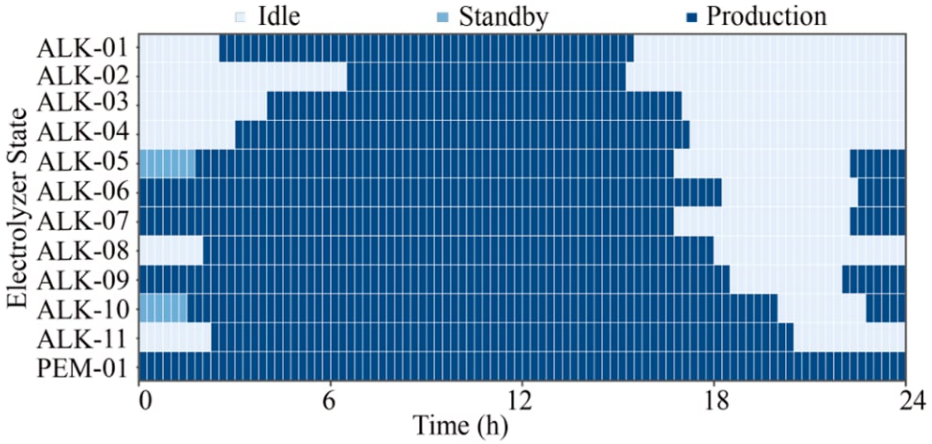

Figure 3. Three-state operating matrix of the electrolyzers in the base case.

The total operating-stress index was 1.1641. The ALK power-variation component was 0.7535, accounting for 64.73% of the total stress. The ALK startup, shutdown, and low-load components were 0.2865, 0.0955, and 0.0114, respectively. The PEM power-variation and high-load components were 0.0142 and 0.0030. Overall, the base-case operating stress was dominated by power variation and switching in the ALK cluster.

4.3. Effects of Operating-Model Features on Capacity and Scheduling

Five cases are used to examine the effects of standby operation, the operating-stress objective, and technology-specific stress weights. B1 is the complete model. B2 sets the operating-stress objective weight to zero and retains all operating constraints. B3 removes the standby state. B4 replaces the technology-specific stress weights with common ALK/PEM values of 19, 6.5, 12.5, and 7.5 for startup, shutdown, power variation, and low-/high-load operation, respectively. B5 repeats B1 to test solution repeatability. All cases were solved with MIP gaps below 1.0×10^{-5}. The capacity and operating results of cases B1–B5 are summarized in Table 4.

Table 4. Comparison of operating-model cases B1–B5.

Case	ALK/PEM Units	Capacity (MW)	$H_{2,year}$ (10^6 kg)	C_{ann} (10^7 CNY yr^{-1})	$LCOH_{el}$ (CNY kg^{-1})	Curtailment (MWh)	ALK Startups	Standby Time (unit·h)	Power Variation (MW)	Stress Index
B1	11/1	56	4.9686	1.33477	2.6864	1791.24	4015	1186.25	85,169.1	1.1641
B2	11/1	56	4.9712	1.33477	2.6850	1791.24	4015	547.50	223,745.0	2.7819
B3	11/1	56	4.9718	1.42237	2.8609	1791.24	4745	0	84,950.1	1.2280
B4	11/1	56	4.9686	1.33477	2.6864	1791.24	4015	1186.25	85,169.1	0.7588
B5	11/1	56	4.9686	1.33477	2.6864	1791.24	4015	1186.25	85,169.1	1.1641

Note: The B2 stress index was evaluated after optimization using the B1 stress definition. B4 uses a common stress-weight scale, and the B1–B4 comparison focuses on stress composition and regulation allocation. B5 is included only to verify repeatability. Wind-power utilization was 99.36% in all cases and is omitted from the table.

All five cases selected 11 ALK units and one PEM unit, corresponding to a total capacity of 56 MW. Under the tested conditions, standby operation, the operating-stress objective, and the stress-weight formulation primarily reshaped unit scheduling; installed capacity remained unchanged across cases.

Comparing B1 with B3 shows that standby reduces equivalent annual ALK startups from 4745 to 4015 (15.38%) and introduces 1186.25 unit·h of standby operation. The combined annualized investment and fixed O&M cost is 8,529,654.62 CNY yr^{-1} in each case. Under the assumed switching costs, startup/shutdown cost decreases from 5,694,000 to 4,818,000 CNY yr^{-1}; this 876,000 CNY yr^{-1} reduction exactly accounts for the change in Cann from 14,223,654.62 to 13,347,654.62 CNY yr^{-1}. The corresponding electrolyzer-side LCOHel decreases from 2.8609 to 2.6864 CNY kg^{-1}. This economic difference is conditional on the assumed transition costs.

The B1–B2 comparison isolates the effect of the operating-stress objective. Capacity, ALK startups, curtailment, and technology-aggregate dispatch are nearly unchanged, but annualized unit-level power variation rises from 85,169.1 to 223,745.0 MW when the stress weight is removed. In B2, the technology-aggregate total variation is only 86,373.6 MW; the unit-level value is 2.59 times larger because equivalent units counter-redistribute power. The stress term therefore removes a scheduling degeneracy and produces a smoother unit allocation. This result quantifies a scheduling effect; physical degradation and lifetime benefits were not estimated.

The B1–B4 comparison shows how technology-specific weights redistribute regulation. Overall capacity, switching, standby time, and total power variation remain nearly unchanged. ALK power variation decreases from 82,979.1 to 79,212.3 MW; PEM power variation increases from 2190.0 to 5956.8 MW. The technology-specific weighting therefore shifts part of the regulating duty from ALK to PEM. B1 and B5 produced identical results, confirming repeatability under the same settings.

Overall, standby primarily reduces ALK switching under the assumed transition costs, and the stress objective suppresses unnecessary unit-level redispatch. Technology-specific weights redistribute regulation between ALK and PEM. These are optimization and scheduling effects; experimental degradation validation remains outside the scope of this study.

Figure 4 summarizes the effects of the five operating-model cases on installed capacity, switching and standby operation, unit-level power variation, and operating-stress composition.

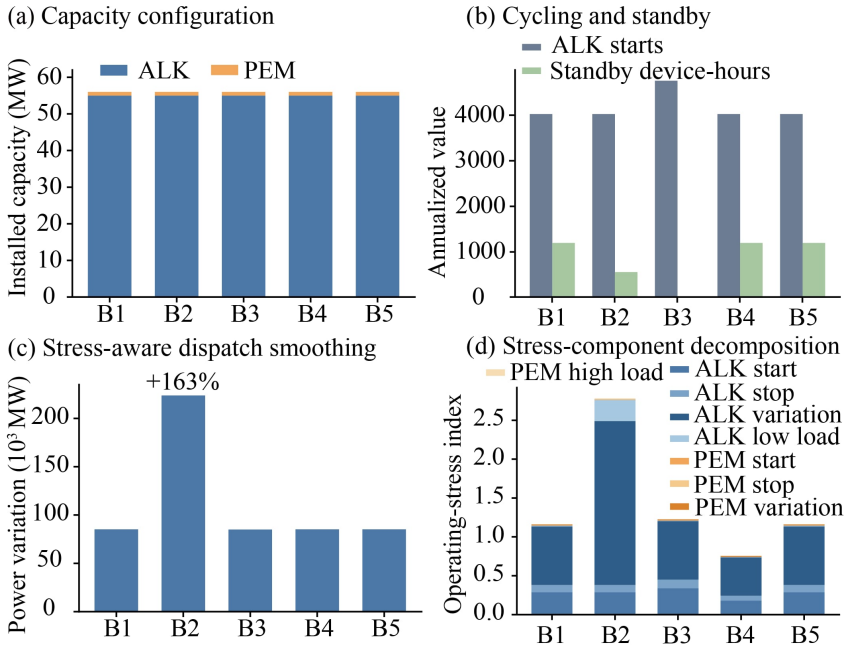

Figure 4. Comparison of operating-model cases: (**a**) ALK and PEM capacities; (**b**) ALK startups and standby time; (**c**) equivalent annual unit-level power variation; and (**d**) operating-stress components. B4 uses common stress weights, so its absolute stress scale differs from those of the other cases and is used only to examine stress composition and regulation allocation.

4.4. Technology Comparison at the Same Hydrogen Production Target

Three technology routes were compared at the same hydrogen-production target: ALK-only (E1), PEM-only (E2), and free configuration (E3). Their maximum feasible equivalent annual hydrogen outputs were 4.9948×10^6, 5.1389×10^6, and 5.1389×10^6 kg, respectively. To maintain a common feasibility margin, the target was set to 98% of the smallest maximum output:

$$H_{2,\mathrm{tar}} = 0.98 \min\left(H_{2,\max}^{E1}, H_{2,\max}^{E2}, H_{2,\max}^{E3}\right) = 4.8949 \times 10^6 \text{ kg} \quad (82)$$

A two-stage procedure was used to reduce differences among near-optimal schedules. Stage 1 minimized the original weighted objective and obtained Φ^*. In Stage 2, the installed capacity was fixed and the original objective was constrained by $\Phi \le \Phi^* + \max(\varepsilon_{\mathrm{abs}}, \varepsilon_{\mathrm{rel}}|\Phi^*|)$, where $\varepsilon_{\mathrm{abs}} = 1.0 \times 10^{-6}$ and $\varepsilon_{\mathrm{rel}} = 1.0 \times 10^{-5}$. Dispatch was then determined lexicographically by minimizing curtailment, operating stress, and startups. After the first two subproblems, the corresponding optimum g^* was retained within $g \le g^* + \max(\varepsilon_{\mathrm{lex,abs}}, \varepsilon_{\mathrm{lex,rel}} \max(1, |g^*|))$, where $\varepsilon_{\mathrm{lex,abs}} = 1.0 \times 10^{-7}$ and $\varepsilon_{\mathrm{lex,rel}} = 1.0 \times 10^{-8}$. The optimization results for the three technology routes at the common hydrogen-production target are summarized in Table 5.

Table 5. Optimization results for the three technology routes at the same hydrogen target.

Route	ALK/PEM Units	Capacity (MW)	$H_{2,\mathrm{year}}$ (10^6 kg)	C_{ann} (10^7 CNY yr^{-1})	$LCOH_{\mathrm{el}}$ (CNY kg^{-1})	Curtailment (MWh)	Startups	Power Variation (MW)	Stress Index
E1 ALK-only	11/0	55	4.89539	1.28602	2.6270	5264.34	4015	75,749.33	1.102543
E2 PEM-only	0/43	43	4.89539	2.46086	5.0269	13,093.83	14,600	70,286.73	0.474507
E3 Free configuration	11/0	55	4.89539	1.28602	2.6270	5264.34	4015	75,749.33	1.102543

Note: The equivalent annual hydrogen outputs of E1, E2, and E3 were 4,895,386.849, 4,895,386.848, and 4,895,386.849 kg yr^{-1}, respectively, with relative deviations from the common target below 1.0×10^{-4}. The Stage 2 curtailment subproblems for E1 and E3 terminated with MIP gaps of 0.452% and 0.469%, respectively; therefore, the reported curtailment values are treated as near-optimal at the stated precision.

All three routes produced approximately 4.89539×10^6 kg yr^{-1}. E1 installs 55 MW of ALK capacity, whereas E2 requires 43 MW of PEM capacity. Although PEM requires less rated capacity because of its operating range and hydrogen-production coefficient, its annualized electrolyzer cost reaches 24.61 million CNY yr^{-1}, 91.4% above the ALK-only value. Its LCOH is correspondingly higher, at 5.0269 CNY kg^{-1} compared with 2.6270 CNY kg^{-1} for E1.

The ALK-only route also uses more wind energy under the present settings. E1 utilizes 98.105% of available wind energy and curtails 5264.34 MWh yr^{-1}, whereas E2 utilizes 95.286% and curtails 13,093.83 MWh yr^{-1}. In this case, PEM's modeled operating flexibility was not associated with higher wind-power utilization.

PEM nevertheless exhibits a lower operating-stress index and lower unit-level power variation. Its annual startup count, however, reaches 14,600 compared with 4015 for ALK. The two technologies therefore show different tradeoffs among cost, wind-power utilization, switching, and operating stress.

The unrestricted case E3 selects 55 MW of ALK and no PEM and reproduces the E1 result. Under a fixed hydrogen-production requirement and the baseline parameters, the model therefore favors an ALK-only configuration.

This differs from the 55 MW ALK/1 MW PEM solution in Section 4.2 because the two cases solve different problems. The base case jointly optimizes hydrogen production, economics, curtailment, and operating stress, whereas Section 4.4 fixes hydrogen output. Removing the marginal value of additional hydrogen production eliminates the 1 MW PEM unit.

Overall, at the common hydrogen target, ALK provides lower hydrogen cost and higher wind-power utilization, whereas PEM provides a lower operating-stress index at substantially higher cost. The unrestricted model consequently selects the ALK-only route.

4.5. Hybrid-Configuration Mechanisms and Sensitivity Analysis

To determine why a small PEM capacity appears in the base case, five sensitivity groups are examined: PEM capital cost, PEM technical characteristics, PEM module size, wind-power variability, and multi-objective weights. Unless otherwise stated, all other parameters and model settings remain unchanged.

4.5.1. PEM Investment Cost

PEM capital cost strongly affects the optimal capacity mix, as shown in Figure 5. At 1.0 and 1.2 times the baseline cost, the solution remains 55 MW ALK/1 MW PEM. Reducing the multiplier to 0.8 increases PEM capacity to 2 MW. At 0.6, the mix changes to 50 MW ALK/6 MW PEM. Further reductions to 0.4 and 0.3 lead to 5 MW ALK/43 MW PEM and a 48 MW PEM-only solution, respectively.

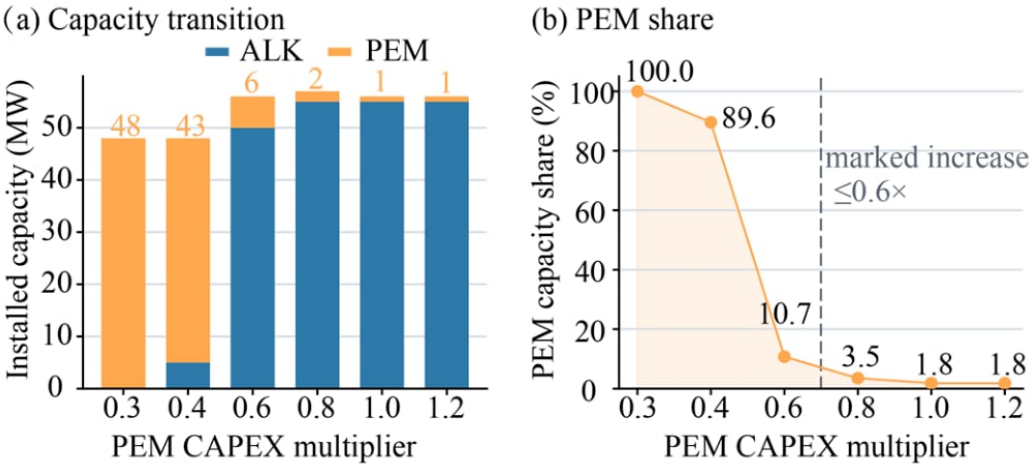

Figure 5. Sensitivity of the optimal configuration to PEM investment cost: installed ALK and PEM capacities (**a**) and PEM capacity share (**b**). The shaded area in panel (**b**) represents the PEM capacity share.

PEM participation therefore increases stepwise as its cost declines. Within the tested discrete values, a pronounced shift occurs around 0.6 times the baseline cost, and PEM becomes dominant at 0.4 or below. The case at 0.6 reaches the 3600 s time limit with the reported MIP gap of 7.72×10^{-5}.

4.5.2. PEM Technical Characteristics

Four cases are used to examine whether the 1 MW PEM capacity is caused by a specific technical advantage. The PEM hydrogen-production coefficient, minimum production load, and maximum operating-power factor are first replaced individually by the corresponding ALK values and then equalized simultaneously.

As shown in Figure 6, all four cases retain the 55 MW ALK/1 MW PEM configuration. Equalizing only the hydrogen-production coefficient resulted in 4.9646×10^6 kg yr^{-1} of hydrogen production and $LCOH_{el} = 2.6886$ CNY kg^{-1}. Equalizing the minimum production load increased annualized curtailment to 1798.54 MWh. In the separate maximum-power-factor case, setting the PEM factor to 1.0 increased curtailment to 2012.97 MWh. When all

three characteristics were equalized, hydrogen production was 4.9601×10^6 kg yr^{-1} and curtailment reached 2020.28 MWh.

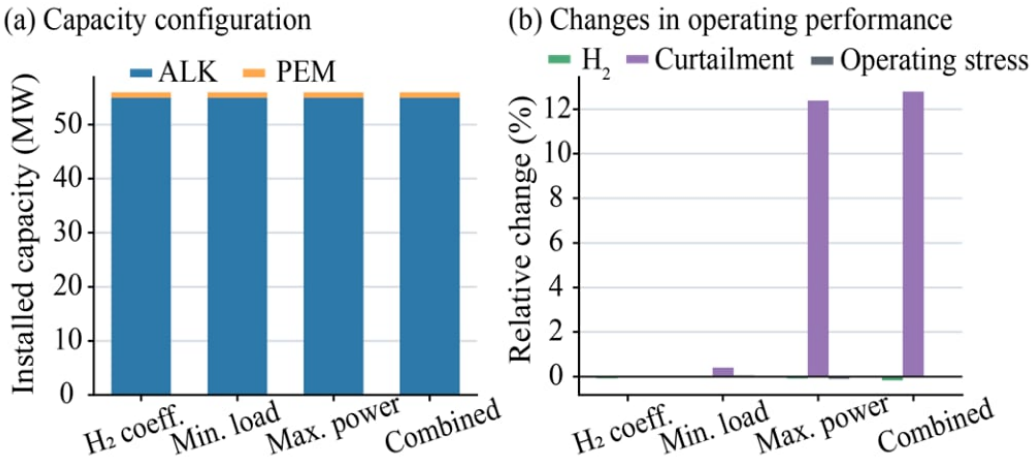

Figure 6. Influence of PEM technical characteristics on the optimization results: installed capacity (**a**) and relative changes in operating-performance indicators (**b**).

Across the tested cases, equalizing the PEM hydrogen-production coefficient, minimum load, and maximum operating-power factor individually or jointly retained the 55 MW ALK/1 MW PEM configuration.

4.5.3. PEM Module Size

The PEM module size is varied; its cost per MW, fixed O&M cost per MW, and technical characteristics remain unchanged. The candidate-unit limit is adjusted in each case so that the maximum available PEM capacity remains 60 MW.

As shown in Figure 7, module size strongly influenced whether PEM entered the optimal configuration. With a 1 MW PEM module, the model selected 1 MW of PEM capacity. Increasing the module size to 2 MW and 2.5 MW still resulted in one PEM unit, corresponding to 2 MW and 2.5 MW, respectively. Curtailment decreased from 1791.24 MWh to 893.34 MWh and 630.08 MWh, whereas $LCOH_{el}$ increased to 2.7734 and 2.8188 CNY kg^{-1}. When the PEM module size reached 5 MW, equal to that of ALK, PEM was no longer selected, and the solution became a 55 MW ALK-only configuration.

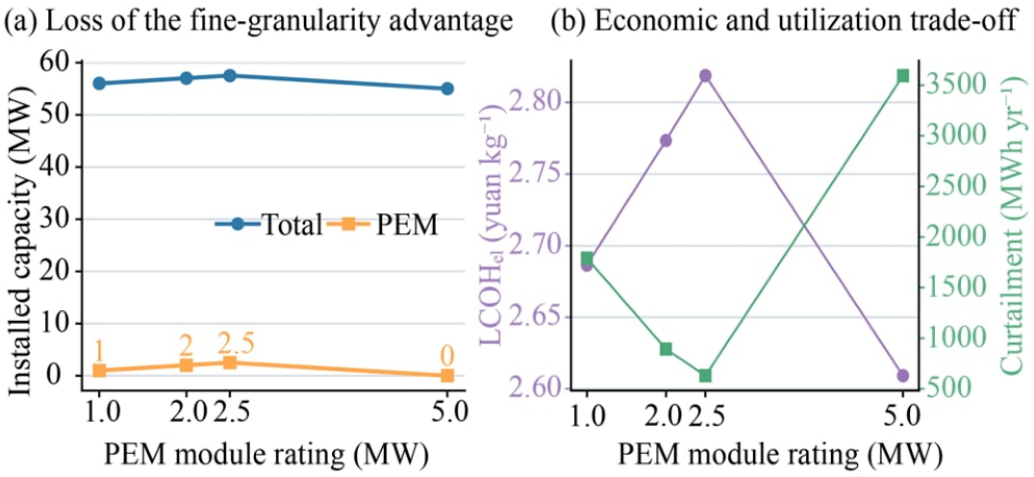

Figure 7. Influence of PEM module-size granularity on the optimization results: total and PEM installed capacity (**a**), and electrolyzer-side LCOH and wind curtailment (**b**).

These results associate the small baseline PEM share with module-size granularity under the tested assumptions. When both technologies use 5 MW modules, the unit-level model selects 55 MW ALK and no PEM. Section 4.7 reports a separate exploratory 1 MW/1 MW comparison using an aggregate formulation. Its result has a different evidential status from the unit-level comparisons in this section.

4.5.4. Wind Power Variability

Five wind scenarios with variability factors of 0.50, 0.75, 1.00, 1.25, and 1.50 were constructed while preserving the total wind energy of the baseline day. Their total power variations were 120.93, 181.40, 241.86, 253.63, and 255.90 MW, respectively. As shown in Figure 8, the corresponding ALK/PEM capacities were 45/0, 50/0, 55/1, 60/0, and 60/0 MW.

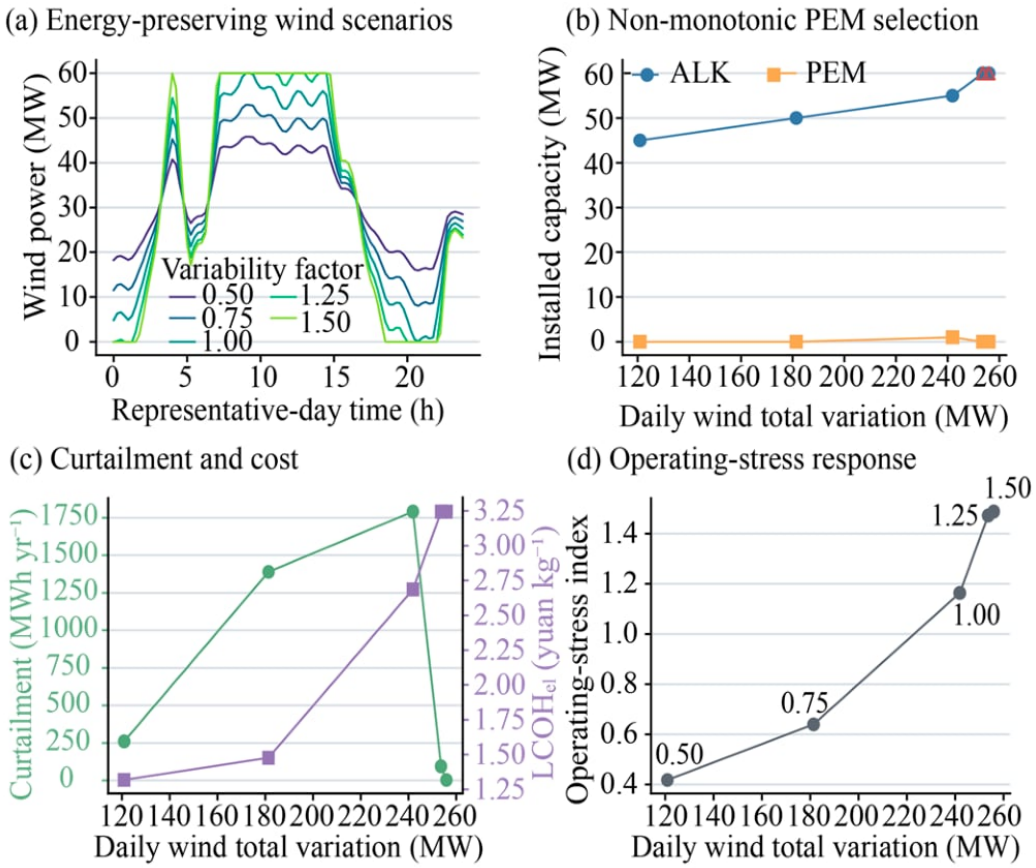

Figure 8. Sensitivity to wind-power variability: wind-power profiles (**a**), installed ALK/PEM capacities (**b**), wind curtailment and electrolyzer-side LCOH (**c**), and operating-stress response (**d**).

Each profile is generated by scaling deviations from the mean wind power and then adjusting the sequence within the 0–60 MW bounds to preserve total energy. Values outside these bounds are clipped, and the remaining energy difference is redistributed among periods with available margin.

The corresponding optimal ALK/PEM capacities are 45/0, 50/0, 55/1, 60/0, and 60/0 MW. Across the constructed scenarios, operating stress generally rises from 0.4184 to 1.4885, whereas PEM capacity follows a non-monotonic pattern.

For variability factors of 1.25 and 1.50, the initial solutions select 60 MW of ALK, equal to the original candidate limit. Expanding the ALK candidate set to 70 and 80 MW leaves the optimal solution and performance metrics unchanged, confirming that the 60 MW ALK solution is not caused by the original bound.

The non-monotonic PEM response indicates that its capacity value depends on the temporal wind profile and the associated system constraints and objectives. Capacity selection depends on the temporal wind profile together with minimum-load constraints, curtailment, stress, and system economics.

4.5.5. Multi-Objective Weights

Five combinations of cost, curtailment, and operating-stress weights were tested to assess the sensitivity of the ALK/PEM capacity mix to local preference changes around the baseline weights of 0.90/0.05/0.05. The model formulation, technical and economic parameters, and 96-point baseline operating day were unchanged. The results are summarized in Table 6.

Table 6. Results of the multi-objective weight-sensitivity test.

Case	w_C /w_{curt}/w_D	ALK/PEM Capacity (MW)	$LCOH_{el}$ (CNY kg^{-1})	Curtailment (MWh)	Operating Stress
W1	0.90/0.05/0.05	55/1	2.686426	1791.2375	1.164106
W2	0.85/0.10/0.05	55/1	2.686426	1791.2375	1.164106
W3	0.85/0.05/0.10	55/2	2.774566	893.3375	1.132491
W4	0.80/0.10/0.10	55/2	2.774566	893.3375	1.132491
W5	0.95/0.025/0.025	55/1	2.685509	1791.2375	1.192752

Note: W1, W2, and W5 reached OPTIMAL status. W3 and W4 returned the best feasible solutions within the 3600 s time limit, with MIP gaps of 1.90×10^{-5} and 2.13×10^{-5}, respectively, and both satisfied all model constraints in the post-solution feasibility check. Objective values are specific to each weight combination and are therefore not compared across cases.

W1 and W2 retained the baseline configuration of 55 MW ALK and 1 MW PEM with the same main performance metrics. W5 also retained this capacity, with $C_{ann} = 1.33477 \times 10^7$ CNY yr^{-1}, equivalent annual hydrogen production of 4.9703×10^6 kg, and an operating-stress index of 1.1928. Thus, for the tested cases with $w_D \leq 0.05$, objective-weight changes mainly reshaped scheduling; the 55 MW ALK/1 MW PEM capacity configuration remained stable.

When the operating-stress weight increased to 0.10, the best feasible W3 and W4 solutions selected 55 MW of ALK and 2 MW of PEM. Equivalent annual hydrogen production increased to 4.9864×10^6 kg, C_{ann} reached 1.38351×10^7 CNY yr^{-1}, curtailment decreased to 893.3375 MWh, and operating stress fell to 1.1325.

The weight test indicates local preference sensitivity: W1, W2, and W5 retained 55 MW ALK/1 MW PEM; the best feasible W3 and W4 solutions within the time limit contained 55 MW ALK/2 MW PEM.

4.5.6. Formation of the Hybrid Configuration

The preceding tests clarify the origin of the hybrid solution. Lower PEM capital cost increases its capacity stepwise and can eventually make PEM dominant. Equalizing its hydrogen-production coefficient, minimum load, and maximum operating power with ALK leaves the 1 MW PEM unit in the solution, indicating that no single tested operating characteristic accounts for the baseline hybrid configuration.

Module-size granularity has a direct effect in the tested cases. When the PEM module size increases from 1 to 5 MW, matching ALK, PEM disappears from the selected configuration. The 1 MW module therefore provides a finer discrete capacity increment than the 5 MW ALK units. Wind variability changes the selected mix non-monotonically, and the best feasible higher-stress-weight solutions also contain more PEM capacity.

Under the baseline conditions, the lower capital cost of ALK makes it the dominant technology, whereas the smaller PEM module allows a limited amount of additional capacity to improve the overall tradeoff. The weight-sensitivity results add a preference dimension: W1, W2, and W5 retained 55 MW ALK/1 MW PEM, while the best feasible W3 and W4 solutions within the time limit selected 55 MW ALK/2 MW PEM. The hybrid configuration therefore reflects capital cost, module size, operating characteristics, wind profile, and objective preferences; its applicability is limited to the conditions examined here.

4.6. Continuous Full-Year Rolling-Horizon Validation

The baseline-day analysis provides a controlled comparison and is complemented by chronological operation to assess cross-day transitions. A continuous full-year simulation evaluates scheduling conclusions under chronological operation. The installed capacity is fixed at 55 MW ALK and 1 MW PEM. Results in this section validate operation at fixed capacity; annual capacity selection and physical degradation are outside its scope.

4.6.1. Data and Computational Settings

The validation uses a normalized project wind sequence containing 35,040 points at 15 min resolution. Small negative values are clipped to zero, changing annual wind energy by only 0.0774%.

Two operating models are compared. L1 includes production, standby, and idle; L2 includes production and idle. At the start of the year, all installed units are idle with zero production power and have satisfied the minimum idle time. A 7 d rolling horizon transfers terminal states, powers, and ALK minimum-idle memory. Each window assumes perfect knowledge of wind over that window; forecast errors are not modeled. The year contains 52 complete 7 d windows and one final 24 h window, with a free terminal state. Section 4.7 reports exploratory 3/7/14 d window comparisons using an aggregate formulation on a common 42 d segment.

The maximum MIP gaps are 9.885×10^{-6} for L1 and 9.945×10^{-6} for L2. Each window uses the baseline objective weights and fixed normalization references. Annual performance metrics are calculated from the complete full-year trajectory.

4.6.2. Full-Year Operating Performance

Table 7 compares L1 and L2 under the same installed capacity and wind input. L1 produced 3.074972×10^6 kg of hydrogen, 0.05% below L2. Wind-power utilization increased from 99.155% to 99.429%, and curtailment decreased from 1455.72 to 983.38 MWh, a reduction of 32.45%. The higher wind-power utilization of L1 includes additional wind energy absorbed during standby operation.

Standby had the largest effect on ALK switching. Relative to L2, L1 reduced ALK startups from 1877 to 1328 (29.25%) and shutdowns from 1872 to 1317 (29.65%). Including PEM, total startups decreased from 2113 to 1561, a reduction of 26.12%. The three-state model mainly kept ALK units in standby during short low-wind periods, thereby avoiding repeated idle–startup transitions.

With the switching-cost settings in Table 2, fewer switching events reduced C_{ann} from 10,840,004.62 to 10,179,254.62 CNY yr^{-1}, or by 6.10%. $LCOH_{el}$ decreased by 6.05%, from 3.52345 to 3.31036 CNY kg^{-1}. Under the assumed cost structure, reduced switching was the main driver of the economic improvement associated with standby operation.

Table 7. Full-year results of the three-state and two-state operating models.

Metric	L1 Three-State Model	L2 Two-State Model	L1 Relative to L2
ALK/PEM capacity (MW)	55/1	55/1	Fixed
Annual hydrogen production (10^6 kg)	3.074972	3.076529	−0.05%
Wind-power utilization (%)	99.429	99.155	+0.274 percentage points
Annual curtailment (MWh)	983.38	1455.72	−32.45%
ALK startups	1328	1877	−29.25%
ALK shutdowns	1317	1872	−29.65%
PEM startups	233	236	−1.27%
PEM shutdowns	232	235	−1.28%
Standby time (unit·h)	3801.00	0	–
Total unit-level power variation (MW)	62,990.84	59,139.07	+6.51%
Total operating stress	0.689257	0.703546	−2.03%
C_{ann} (CNY yr^{-1})	10,179,254.62	10,840,004.62	−6.10%
$LCOH_{el}$ (CNY kg^{-1})	3.31036	3.52345	−6.05%

4.6.3. Operating-Stress Components

Standby reduces the total operating-stress index from 0.703546 to 0.689257, a decrease of 2.03%. The main reductions occur in ALK startup stress, from 0.133918 to 0.094749, and shutdown stress, from 0.044521 to 0.031321.

This benefit is partly offset by greater within-operation adjustment. ALK power-variation stress increases from 0.478843 to 0.511936, and low-load stress rises from 0.020726 to 0.024556. PEM power-variation and high-load stress also increase slightly. Consistently, total unit-level power variation rises by 6.51%, from 59,139.07 to 62,990.84 MW.

Standby therefore changes the composition of operating stress: some shutdown–restart cycles are replaced by additional power adjustment and low-load operation. The reduction in switching stress also lowers the total index.

4.6.4. Comparison with Representative-Day Annualization

The continuous full-year results differ markedly from values obtained by multiplying the representative day by 365. The representative-day profile corresponds to 277,777.78 MWh of annualized wind energy, 61.31% above the 172,200.50 MWh in the full-year sequence. Differences in hydrogen production and economic results therefore reflect both resource level and temporal distribution.

The discrepancy is larger for transition-dependent metrics. For the three-state model, representative-day annualization gives 4015 ALK startups, 202.33% above the full-year result of 1328. Its operating-stress index is 68.89% higher, whereas annualized standby time is 68.79% lower. Similar differences occur for the two-state model. Moreover, the representative-day base case contains no PEM startups, whereas the continuous simulations produce 233 and 236 PEM startups for L1 and L2.

These results show that startup counts, standby duration, and operating stress depend strongly on the temporal sequence and boundary treatment. Representative-day annualization therefore provides a controlled benchmark for comparing configurations and modeling choices; annual switching-frequency prediction requires chronological data.

Despite the difference in absolute annual metrics, the fixed-capacity full-year simulation supports one scheduling conclusion: under the assumed transition costs, standby reduces ALK switching and lowers the reported operating-stress proxy and electrolyzer-side cost. The simulation evaluates scheduling at the fixed baseline capacity; physical degradation and full-year capacity selection remain outside its scope.

4.7. Exploratory Aggregate Screening and Model Boundaries

The following additional calculations use an aggregate screening formulation with integer counts of units in each state. Its power-variation term is the absolute change in total production power for each technology, and its load-deviation terms are calculated from technology-level power and production-state counts. These terms differ from the unit-level sums in Section 2.4: opposing unit adjustments can cancel after aggregation. Agreement with Section 4.2 baseline summaries alone is therefore insufficient to establish formulation equivalence. Table 8 reports exploratory aggregate-model results; they provide hypotheses for further unit-level testing, with no claim that they establish robustness of the original MILP. The unit-level results in Sections 4.2–4.6 are unchanged.

Table 8. Exploratory aggregate-model results (separate from unit-level validation).

Check	Range or Setting	Capacity Result	Interpretation
Stress coefficients	Each coefficient: 0.5/1.0/1.5×	55/1 MW in all cases	Aggregate-model outcome
Stress thresholds	ALK: 0.25–0.40; PEM: 1.00–1.10 p.u.	55/1 MW in all cases	Aggregate-model outcome
Matched modules	1/1 MW and 5/5 MW	57/0 and 55/0 MW	Different aggregation levels
Four representative days	Weights: 123/89/84/69 d	40/0 MW	Aggregate scenario screening
Hydrogen price	10/20/30 CNY kg^{-1}	55/0, 55/1, 55/2 MW	Aggregate economic screening
Switching costs	0.5/1.0/1.5×	55/1 MW in all cases	Aggregate cost screening
Rolling horizon	3/7/14 d; fixed 42 d segment	Capacity fixed at 55/1 MW	Aggregate window screening

First, each of the eight relative stress weights was varied individually to 0.5 and 1.5 times its baseline value in the aggregate formulation. All 16 screening cases selected 55 MW ALK/1 MW PEM; hydrogen production ranged from 4.9673×10^6 to 4.9696×10^6 kg and electrolyzer-side LCOH from 2.6859 to 2.6871 CNY kg^{-1}. Annualized cost and curtailment were 13,347,654.62 CNY yr^{-1} and 1791.24 MWh. The aggregate stress index ranged from 0.7850 to 1.5384 as its weights changed. Threshold screening used ALK values of 0.25, 0.30, 0.35, and 0.40 p.u. and PEM values of 1.00, 1.05, and 1.10 p.u., including their baseline settings; the selected capacity remained 55/1 MW. These outcomes describe local behavior of the aggregate approximation. Unit-level robustness and physical calibration remain separate validation requirements.

Second, the aggregate 1 MW/1 MW module comparison retained technology-specific operating parameters and per-MW CAPEX/O&M, with ALK transition costs scaled per MW, and selected 57 MW ALK and no PEM. The unit-level 5 MW/5 MW comparison in Section 4.5.3 selected 55 MW ALK and no PEM. Because the two calculations use different aggregation levels, only the latter directly supports the original model; the 1 MW/1 MW outcome remains exploratory.

Third, the 35,040-point wind sequence was divided into 365 daily profiles and clustered by deterministic k-means on unscaled 96-point MW profiles (seed 1; 20 iterations). Four centroid profiles with weights of 123, 89, 84, and 69 d preserve the source energy of 172,200.50 MWh. Independent daily cyclic boundaries and shared capacity were used in the aggregate screening, which selected 40 MW ALK and no PEM. Centroid averaging smooths intraday variability, and independent cycles omit interday chronology. Energy preservation alone therefore provides limited evidence about switching behavior. This capacity is an aggregate-screening outcome, with annual chronological capacity optimality left unresolved.

Fourth, aggregate economic screening used hydrogen prices of 10, 20, and 30 CNY kg^{-1} and selected ALK/PEM capacities of 55/0, 55/1, and 55/2 MW, with electrolyzer-side LCOH values of 2.6106, 2.6864, and 2.7731 CNY kg^{-1} and hydrogen outputs of 4.9261×10^6, 4.9686×10^6, and 4.9890×10^6 kg. Multipliers of 0.5, 1.0, and 1.5 on all transition costs retained 55/1 MW; annualized costs were 10,938,654.62, 13,347,654.62, and 15,756,654.62 CNY yr^{-1}, and LCOH values were 2.2016, 2.6864, and 3.1713 CNY kg^{-1}. These are economic scenarios within the aggregate approximation, not market forecasts or verified unit-level sensitivity results.

Finally, the aggregate formulation was used for fixed-capacity 3, 7, and 14 d rolling-window comparisons over one continuous 42 d segment. ALK startups were 119, 116, and 113, and aggregate stress indices were 0.06512, 0.06531, and 0.06533. Relative to 7 d, hydrogen production differed by at most 0.037% and ALK startups by 2.59%. Recorded total solution times were 40.30, 47.29, and 106.41 s; maximum window MIP gaps were 2.48×10^{-5}, 7.66×10^{-6}, and 0, respectively, with a 120 s limit per window. These exploratory comparisons establish neither unit-level window invariance nor forecast robustness. A computational-scaling benchmark and unit-level revalidation remain outstanding.

5. Conclusions

This study developed an approach for the joint optimization of discrete ALK/PEM capacity, unit operating states, and technology-specific operating stress in an off-grid ReP2H system. Module-size granularity is explicitly represented, and the model is evaluated through operating-model comparisons, equal-hydrogen tests, sensitivity analyses, and continuous full-year rolling-horizon simulation. The main findings are as follows:

(1) For the selected high-energy baseline day, the solution contains 55 MW of ALK and 1 MW of PEM, with 99.36% wind-power utilization and an electrolyzer-side LCOH of 2.6864 CNY kg^{-1}. This cost excludes upstream wind generation and downstream balance-of-plant items.

(2) Standby and the operating-stress objective mainly reshape unit scheduling. Under baseline-day annualization, standby reduces ALK startups by 15.38% and the electrolyzer-side LCOH by 6.10% under the assumed switching costs. The unit-level stress term suppresses counter-redispatch among identical units and serves as a scheduling proxy; it has no lifetime calibration.

(3) Under a common hydrogen target, the unrestricted unit-level model selects 55 MW ALK and no PEM. The 5 MW/5 MW module comparison also selects ALK only; PEM participation changes with its capital cost and the objective weights. W1, W2, and W5 retain 55 MW ALK/1 MW PEM, whereas the best feasible W3 and W4 solutions within the time limit contain 55 MW ALK/2 MW PEM. These results associate the baseline PEM share with discrete module size and the tested economic and decision-preference assumptions.

(4) At fixed baseline capacity, the continuous full-year simulation shows that standby reduces ALK startups and shutdowns by 29.25% and 29.65%, respectively; the operating-stress proxy and electrolyzer-side LCOH decrease by 2.03% and 6.05%. These findings concern chronological scheduling under the assumed transition costs. Annual capacity optimality remains unresolved; the aggregate screening in Section 4.7 provides exploratory evidence only.

Overall, ALK is favored under the baseline economic assumptions, and the smaller PEM module provides a finer capacity increment. The selected mix applies to the wind representation, economics, module size, operating assumptions, and objective preferences examined here.

Future work will incorporate load-dependent efficiency, calibrated degradation and transition models, forecast uncertainty, and chronological multi-year capacity optimiza-

tion. Linking the operating-stress proxy to physical lifetime and transferring the reported configuration to other projects will require these extensions.

Author Contributions: Conceptualization, J.Z. and S.L.; methodology, S.L.; software, S.L.; validation, H.H., Z.Z., L.Z., S.X., and Z.Q.; formal analysis, J.Z., J.L., S.L., and Z.Q.; investigation, H.H., Z.Z., L.Z., Y.L., S.X., and Z.Q.; resources, J.Z., H.H., Z.Z., L.Z., J.L., and Y.L.; data curation, L.Z., J.L., Y.L., and S.X.; writing—original draft preparation, S.L.; writing—review and editing, J.Z., H.H., Z.Z., L.Z., J.L., Y.L., S.L., Y.Q., S.X., and Z.Q.; visualization, S.L.; supervision, J.Z., S.L., and Y.Q.; project administration, J.Z., J.L., and Y.Q.; funding acquisition, J.Z. All authors have read and agreed to the published version of the manuscript.

Funding: This research was funded by Key Task 7 of the Central Enterprise Green Hydrogen Production, Storage, and Transportation Innovation Consortium and the Science and Technology Project of Power Construction Corporation of China (DJ-HXGG-2024-05).

Data Availability Statement: Data available on request from the authors.

Conflicts of Interest: Authors Jianguo Zhu, Huimin Hu, Zhiyin Zhang, and Lingwen Zeng were employed by POWERCHINA Hubei Electric Engineering Corporation Limited. Authors Shanshan Xu and Zhicheng Qi were employed by POWERCHINA Beijing Engineering Corporation Limited. The remaining authors declare that the research was conducted in the absence of any commercial or financial relationships that could be construed as potential conflicts of interest. The authors declare that this study received funding from the Technology Project of Power Construction Corporation of China. The funder was not involved in the study design, collection, analysis, interpretation of data, the writing of this article, or the decision to submit it for publication.

Abbreviations

The following abbreviations are used in this manuscript:

ALK	Alkaline electrolyzer
PEM	Proton exchange membrane electrolyzer
MILP	Mixed-integer linear programming
LCOH	Levelized cost of hydrogen
O&M	Operation and maintenance
Nomenclature	
Symbol	Definition
C_{ann}	Annualized electrolyzer-side investment, fixed O&M, and transition cost
C_{net}	Annualized electrolyzer-side cost less hydrogen revenue
R_{H2}	Hydrogen revenue
$LCOH_{el}$	Electrolyzer-side cost per unit of hydrogen
$H_{2,year}$	Annual or equivalent annual hydrogen production
E_W	Available wind energy over the optimization horizon
E_{curt}	Wind energy curtailed over the optimization horizon
D_{sys}	Fixed-reference relative operating-stress index
D_{ref}	Fixed system reference used to normalize operating stress
P_{ref}	Fixed reference power
C_{ref}	Cost-normalization reference scale
w_C, w_{curt}, w_D	Cost, curtailment, and operating-stress objective weights
Δt	Scheduling interval

References

1. Li, J.; Lin, J.; Wang, J.; Lu, X.; Nielsen, C.P.; McElroy, M.B.; Song, Y.; Song, J.; Lyu, X.; Yu, M.; et al. Redesigning Electrification of China's Ammonia and Methanol Industry to Balance Decarbonization with Power System Security. *Nat. Energy* **2025**, *10*, 762–773. [CrossRef]
2. National Development and Reform Commission; National Energy Administration. *Medium- and Long-Term Plan for the Development of the Hydrogen Energy Industry (2021–2035)*; National Development and Reform Commission: Beijing, China, 2022.
3. Writing Group for the Blue Book on the Development of New Power Systems. *Blue Book on the Development of New Power Systems*; China Electric Power Press: Beijing, China, 2023.

4. Carmo, M.; Fritz, D.L.; Mergel, J.; Stolten, D. A comprehensive review on PEM water electrolysis. *Int. J. Hydrogen Energy* **2013**, *38*, 4901–4934. [CrossRef]
5. International Renewable Energy Agency. *Green Hydrogen Cost Reduction: Scaling Up Electrolysers to Meet the 1.5 °C Climate Goal*; IRENA: Abu Dhabi, United Arab Emirates, 2020.
6. Ursúa, A.; Gandía, L.M.; Sanchis, P. Hydrogen production from water electrolysis: Current status and future trends. *Proc. IEEE* **2012**, *100*, 410–426. [CrossRef]
7. Buttler, A.; Spliethoff, H. Current status of water electrolysis for energy storage, grid balancing and sector coupling via power-to-gas and power-to-liquids: A review. *Renew. Sustain. Energy Rev.* **2018**, *82*, 2440–2454. [CrossRef]
8. Sayed-Ahmed, H.; Toldy, Á.I.; Santasalo-Aarnio, A. Dynamic operation of proton exchange membrane electrolyzers—Critical review. *Renew. Sustain. Energy Rev.* **2024**, *189*, 113883. [CrossRef]
9. Qiu, Y.; Zhou, Y.; Chen, S.; Zang, T.; Zhou, B. Flexibility assessment and aggregation of alkaline electrolyzers considering dynamic process constraints for energy management of renewable power-to-hydrogen systems. *Renew. Energy* **2024**, *235*, 121261. [CrossRef]
10. Şahin, M.E. An overview of different water electrolyzer types for hydrogen production. *Energies* **2024**, *17*, 4944. [CrossRef]
11. Jia, C.; Wang, L.; Meng, E.; Yang, D.; Guo, D.; Liu, Y. Optimal capacity configuration and day-ahead scheduling of wind–solar–hydrogen coupled power generation system. *Electr. Power* **2020**, *53*, 80–87.
12. Kang, Z.; Liu, S. Research on capacity optimization configuration of renewable energy off grid hydrogen production system considering collaborative electrolysis. *Energies* **2024**, *17*, 1962. [CrossRef]
13. Geng, Y.; Liu, Q.; Zheng, H.; Yan, S. Two-stage collaborative power optimization for off-grid wind–solar hydrogen production systems considering reserved energy of storage. *Energies* **2025**, *18*, 2970. [CrossRef]
14. Cooper, N.; Horend, C.; Röben, F.; Bardow, A.; Shah, N. A framework for the design & operation of a large-scale wind-powered hydrogen electrolyzer hub. *Int. J. Hydrogen Energy* **2022**, *47*, 8671–8686. [CrossRef]
15. Sharifzadeh, M.; Cooper, N.; Van't Noordende, H.; Shah, N. Operational strategies and integrated design for producing green hydrogen from wind electricity. *Int. J. Hydrogen Energy* **2024**, *64*, 650–675. [CrossRef]
16. Schmidt, O.; Gambhir, A.; Staffell, I.; Hawkes, A.; Nelson, J.; Few, S. Future cost and performance of water electrolysis: An expert elicitation study. *Int. J. Hydrogen Energy* **2017**, *42*, 30470–30492. [CrossRef]
17. Glenk, G.; Reichelstein, S. Economics of converting renewable power to hydrogen. *Nat. Energy* **2019**, *4*, 216–222. [CrossRef]
18. Lin, L.; Li, X.; Ou, K.; Xing, J.; Wang, Y.-X. Mixed integer linear programming-based optimal capacity configuration of ALK/PEM mixed water electrolysis system. *Energy* **2025**, *333*, 137419. [CrossRef]
19. Campbell-Stanway, C.M.; Becerra, V.M.; Radhakrishna Prabhu, S.G. Techno-economic analysis with electrolyser degradation modelling in green hydrogen production scenarios. *Int. J. Hydrogen Energy* **2025**, *106*, 80–95. [CrossRef]
20. Song, J.; Gao, J.; Liang, D.; Li, G.; Deng, Z.; Xu, G.; Zhang, L.; Xie, C.; Xu, C. A review on modeling of hydrogen production system with proton exchange membrane electrolysis. *Electr. Power Constr.* **2024**, *45*, 58–78.
21. Ye, Q.; Song, J.; Hou, K.; Guo, Z.; Xu, G.; Deng, Z.; Li, B. Review of hydrogen permeation in PEM water electrolysis. *Chin. J. Eng.* **2022**, *44*, 1274–1281.
22. Guo, Z.; Zhu, Y.; Ye, Q.; Hu, X.; Song, J.; Xu, G.; Deng, Z.; Duan, F.; Liu, R. Research Progress on the Effect of Ion Pollution on Proton Exchange Membrane Electrolysis for Hydrogen Production. *J. Glob. Energy Interconnect.* **2023**, *6*, 325–330.
23. Qiu, Y.; Zhou, B.; Zang, T.; Zhou, Y.; Chen, S.; Qi, R.; Li, J.; Lin, J. Extended load flexibility of utility-scale P2H plants: Optimal production scheduling considering dynamic thermal and HTO impurity effects. *Renew. Energy* **2023**, *217*, 119198. [CrossRef]
24. David, M.; Ocampo-Martínez, C.; Sánchez-Peña, R. Advances in alkaline water electrolyzers: A review. *J. Energy Storage* **2019**, *23*, 392–403. [CrossRef]
25. Brauns, J.; Turek, T. Alkaline water electrolysis powered by renewable energy: A review. *Processes* **2020**, *8*, 248. [CrossRef]
26. Haug, P.; Koj, M.; Turek, T. Influence of process conditions on gas purity in alkaline water electrolysis. *Int. J. Hydrogen Energy* **2017**, *42*, 9406–9418. [CrossRef]
27. Niu, M.; Li, X.; Sun, C.; Xiu, X.; Wang, Y.; Hu, M.; Dong, H. Operation optimization of wind/battery storage/alkaline electrolyzer system considering dynamic hydrogen production efficiency. *Energies* **2023**, *16*, 6132. [CrossRef]
28. Gambou, F.; Guilbert, D.; Zasadzinski, M.; Rafaralahy, H. A comprehensive survey of alkaline electrolyzer modeling: Electrical domain and specific electrolyte conductivity. *Energies* **2022**, *15*, 3452. [CrossRef]
29. Endrődi, B.; Trapp, C.A.; Szén, I.; Bakos, I.; Lukovics, M.; Janáky, C. Challenges and opportunities of the dynamic operation of PEM water electrolyzers. *Energies* **2025**, *18*, 2154. [CrossRef]
30. Babic, U.; Suermann, M.; Büchi, F.N.; Gubler, L.; Schmidt, T.J. Critical Review—Identifying critical gaps for polymer electrolyte water electrolysis development. *J. Electrochem. Soc.* **2017**, *164*, F387–F399. [CrossRef]
31. Rakousky, C.; Reimer, U.; Wippermann, K.; Carmo, M.; Lüke, W.; Stolten, D. An analysis of degradation phenomena in polymer electrolyte membrane water electrolysis. *J. Power Sources* **2016**, *326*, 120–128. [CrossRef]

32. Chandesris, M.; Médeau, V.; Guillet, N.; Chelghoum, S.; Thoby, D.; Fouda-Onana, F. Membrane degradation in PEM water electrolyzer: Numerical modeling and experimental evidence of the influence of temperature and current density. *Int. J. Hydrogen Energy* **2015**, *40*, 1353–1366. [CrossRef]
33. Frensch, S.H.; Fouda-Onana, F.; Serre, G.; Thoby, D.; Araya, S.S.; Kær, S.K. Influence of the operation mode on PEM water electrolysis degradation. *Int. J. Hydrogen Energy* **2019**, *44*, 29889–29898. [CrossRef]
34. Zhou, B.; Wu, C.; Qiu, Y.; Zang, T.; Zhu, J.; Zhou, Y. Optimal scheduling of multi-electrolyzer power-to-hydrogen clusters considering the temporal uncertainty of photovoltaic power. *Electr. Power Constr.* **2023**, *44*, 108–117.
35. Zeng, Y.; Qiu, Y.; Zhu, J.; Chen, S.; Zhou, B.; Li, J.; Yang, B.; Lin, J. Scheduling multiple industrial electrolyzers in renewable P2H systems: A coordinated active-reactive power management method. *IEEE Trans. Sustain. Energy* **2025**, *16*, 201–215. [CrossRef]
36. Zhu, J.; Qiu, Y.; Zeng, Y.; Zhou, Y.; Chen, S.; Zang, T.; Zhou, B.; Yu, Z.; Lin, J. Exploring the optimal size of grid-forming energy storage in an off-grid renewable P2H system under multi-timescale energy management. *Appl. Energy* **2026**, *407*, 127295. [CrossRef]
37. Zeng, Y.; Qiu, Y.; Xu, L.; Gu, C.; Zhou, Y.; Li, J.; Chen, S.; Zhou, B. Optimal investment portfolio of thyristor- and IGBT-based electrolysis rectifiers in utility-scale renewable P2H systems. *IEEE Trans. Sustain. Energy* **2026**, *17*, 740–755. [CrossRef]
38. Qiu, Y.; Li, J.; Zeng, Y.; Zhou, Y.; Chen, S.; Qiu, X.; Zhou, B.; He, G.; Ji, X.; Li, W. Dynamic modeling and control of multi-stack alkaline water electrolysis systems with shared gas separators and lye circulation: Industrial data-based validation and simulation. *Int. J. Hydrogen Energy* **2026**, *259*, 156155. [CrossRef]
39. Ma, B.; Zheng, J.; Xian, Z.; Wang, B.; Ma, H. Optimal operation strategy for wind–photovoltaic power-based hydrogen production systems considering electrolyzer start-up characteristics. *Processes* **2024**, *12*, 1756. [CrossRef]
40. Cheng, J.; Wang, Y.; Liu, S.; Cheng, X. Coordinated optimization operation strategy for hybrid hydrogen production system considering dynamic characteristics and state transition of electrolyzers. *Energies* **2026**, *19*, 996. [CrossRef]
41. Ling, P.; Wen, C.; Wang, X.; Liu, Q.; Huang, L.; Cao, C.; Tang, C.; Tu, Z. Two-stage optimization for hybrid renewable hydrogen production systems: Capacity configuration and electrolyzer array operation strategy. *Energy* **2026**, *355*, 141127. [CrossRef]
42. Chen, W.; Jiang, Y.; Li, Q. Multi-state optimized operation strategy for multi-electrolyzer hydrogen production system considering wind power uncertainty. *Int. J. Hydrogen Energy* **2026**, *213*, 153782. [CrossRef]
43. Li, Z.; Tu, Z.; Yi, Z.; Xu, Y. Coordinated control of proton exchange membrane electrolyzers and alkaline electrolyzers for a wind-to-hydrogen islanded microgrid. *Energies* **2024**, *17*, 2317. [CrossRef]
44. Li, Y.; Zhou, S.; Pan, G. An Effective Optimisation Method for Coupled Wind–Hydrogen Power Generation Systems Considering Scalability. *Processes* **2023**, *11*, 343. [CrossRef]
45. Yodwong, B.; Guilbert, D.; Hinaje, M.; Phattanasak, M.; Kaewmanee, W.; Vitale, G. Proton Exchange Membrane Electrolyzer Emulator for Power Electronics Testing Applications. *Processes* **2021**, *9*, 498. [CrossRef]
46. Gao, Z.; Tian, Y. Self-Sustaining Control Strategy for Proton-Exchange Membrane Electrolysis Devices Based on Gradient-Disturbance Observation Method. *Processes* **2023**, *11*, 828. [CrossRef]
47. Miličić, T.; Altaf, H.; Vorhauer-Huget, N.; Živković, L.A.; Tsotsas, E.; Vidaković-Koch, T. Modeling and Analysis of Mass Transport Losses of Proton Exchange Membrane Water Electrolyzer. *Processes* **2022**, *10*, 2417. [CrossRef]
48. Rodríguez, J.; Amores, E. CFD Modeling and Experimental Validation of an Alkaline Water Electrolysis Cell for Hydrogen Production. *Processes* **2020**, *8*, 1634. [CrossRef]
49. International Renewable Energy Agency. *Hydrogen from Renewable Power: Technology Outlook for the Energy Transition*; IRENA: Abu Dhabi, United Arab Emirates, 2018.
50. Guo, X.; Li, X.; Xu, Z.; He, G.; Miao, P. Cost Analysis of Hydrogen Production by Electrolysis of Renewable Energy. *Energy Storage Sci. Technol.* **2020**, *9*, 688–695. [CrossRef]
51. Sun, X.; Liu, C.; Niu, X.; Zhao, L. Research on Typical Design of Wind-Solar Coupled Hydrogen Production System. *South. Energy Constr.* **2023**, *10*, 112–119. [CrossRef]
52. Ding, L.; Peng, X.; Hou, J.; Kang, W.; Lyu, H.; Zhang, K.; Hou, C. Hydrogen Production by Proton Exchange Membrane Water Electrolysis in the Presence of Wind-Solar Fluctuating Power Supply: Development and Application. *Strateg. Study CAE* **2023**, *25*, 237–247. [CrossRef]
53. Li, H.; Yu, H.; Wang, H.; Gou, X.; Liu, F.; Li, L.; Wang, Q.; Zhang, X.; Li, Y. Prediction of Hydrogen Consumption Scale and Hydrogen Price Based on LEAP Model and Two-Factor Learning Curve. *Front. Energy Res.* **2024**, *12*, 1450966. [CrossRef]
54. Varela, C.; Mostafa, M.; Zondervan, E. Modeling Alkaline Water Electrolysis for Power-to-X Applications: A Scheduling Approach. *Int. J. Hydrogen Energy* **2021**, *46*, 9303–9313. [CrossRef]

Disclaimer/Publisher's Note: The statements, opinions and data contained in all publications are solely those of the individual author(s) and contributor(s) and not of MDPI and/or the editor(s). MDPI and/or the editor(s) disclaim responsibility for any injury to people or property resulting from any ideas, methods, instructions or products referred to in the content.